ChemPubSoc Europe

DOI: 10.1002/chem.201405129

CHEMISTRY
A European Journal
Full Paper

Transfer Hydrogenation |*Hot Paper*|

# Bio-Inspired Transition Metal–Organic Hydride Conjugates for Catalysis of Transfer Hydrogenation: Experiment and Theory

Alex McSkimming,[a] Bun Chan,[b] Mohan M. Bhadbhade,[c] Graham E. Ball,[a] and Stephen B. Colbran*[a]

**Abstract:** Taking inspiration from yeast alcohol dehydrogenase (yADH), a benzimidazolium ($BI^+$) organic hydride-acceptor domain has been coupled with a 1,10-phenanthroline (phen) metal-binding domain to afford a novel multifunctional ligand ($\mathbf{L}^{BI+}$) with hydride-carrier capacity ($\mathbf{L}^{BI+} + H^- \rightleftharpoons \mathbf{L}^{BI}H$). Complexes of the type $[Cp^*M(\mathbf{L}^{BI})Cl][PF_6]_2$ (M = Rh, Ir) have been made and fully characterised by cyclic voltammetry, UV/Vis spectroelectrochemistry, and, for the $Ir^{III}$ congener, X-ray crystallography. $[Cp^*Rh(\mathbf{L}^{BI})Cl][PF_6]_2$ catalyses the transfer hydrogenation of imines by formate ion in very goods yield under conditions where the corresponding $[Cp^*Ir(\mathbf{L}^{BI})Cl][PF_6]$ and $[Cp^*M(phen)Cl][PF_6]$ (M = Rh, Ir) complexes are almost inert as catalysts. Possible alternatives for the catalysis pathway are canvassed, and the free energies of intermediates and transition states determined by DFT calculations. The DFT study supports a mechanism involving formate-driven Rh–H formation (90 kJ mol$^{-1}$ free-energy barrier), transfer of hydride between the Rh and $BI^+$ centres to generate a tethered benzimidazoline (BIH) hydride donor, binding of imine substrate at Rh, back-transfer of hydride from the BIH organic hydride donor to the Rh-activated imine substrate (89 kJ mol$^{-1}$ barrier), and exergonic protonation of the metal-bound amide by formic acid with release of amine product to close the catalytic cycle. Parallels with the mechanism of biological hydride transfer in yADH are discussed.

## Introduction

Nature rarely uses molecular hydrogen for hydrogenation reactions.[1] Rather, throughout terrestrial life, the nucleotide-substituted nicotinamides NAD(P)H are used to carry and transfer hydride regio- and enantioselectively to an unsaturated substrate bound and hence activated within the active site of a (de)hydrogenase enzyme.[2] In metallodehydrogenases, a metal ion serves as the substrate binding and activating site.[3] Examples are the mononuclear zinc centre in yeast alcohol dehydrogenase (yADH) for reduction of acetaldehyde to ethanol by NADPH in the terminal step of yeast fermentation (see below, Scheme 2a),[3c] and the dinuclear magnesium centre for the reduction of either 2-acetolactate or 2-aceto-2-hydroxybutyrate by NADPH catalysed by acetohydroxy acid isomeroreductase in the biosynthesis of the essential branched-chain amino acids (isoleucine, leucine and valine).[3d,e]

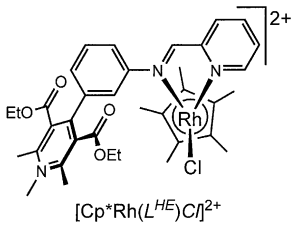


**Scheme 1.** Hantzsch pyridinium ($HE^+$)–rhodium conjugate $[Cp^*Rh(\mathbf{L}^{HE})Cl]^{2+}$, previously used to catalyse transfer hydrogenation of imines.[4,5]

Inspired by biology, we recently demonstrated that a careful combination of abutted co-facing organic hydride and metal centres in one complex led to an efficient catalyst for transfer hydrogenation. We used the Hantzsch pyridinium ($HE^+$)–rhodium conjugate $[Cp^*Rh(\mathbf{L}^{HE})Cl]^{2+}$ (Scheme 1) as the catalyst for transfer hydrogenation of imine substrates in air, at ambient temperature, by 1:1 formic acid/sodium formate.[4,5] Subsequent study revealed that the pyridylimine ligand used to anchor the Hantzsch pyridinium group to the metal is unstable under the catalytic conditions and slowly hydrolyses, thus limiting the catalyst lifetime.[6] Therefore, to increase the catalyst lifetime, an organic hydride donor-substituted chelate ligand with increased stability over the Hantzsch-substituted pyridylimine ligand previously studied was sought.

We describe herein the first multifunctional chelate ligand ($\mathbf{L}^{BI}H$) with a benzo[*d*]imidazoline organic hydride-donor domain (Scheme 2b and Scheme 3). Ligand $\mathbf{L}^{BI}H$ has the fol-

[a] *A. McSkimming, Dr. G. E. Ball, Prof. S. B. Colbran*
*School of Chemistry, The University of New South Wales*
*Sydney, NSW 2052 (Australia)*
*E-mail: s.colbran@unsw.edu.au*

[b] *Dr. B. Chan*
*School of Chemistry, The University of Sydney*
*Sydney, NSW 2006 (Australia)*

[c] *Dr. M. M. Bhadbhade*
*Mark Wainwright Analytical Centre, The University of New South Wales*
*Sydney, NSW 2052 (Australia)*

*Supporting information for this article is available on the WWW under http://dx.doi.org/10.1002/chem.201405129.*

lowing design features: a) A 1,10-phenanthroline metal-binding domain, employed because it is a robust chelate ligand, easily and diversely derivatised, that strongly complexes a wide variety of metal ions;[7–9] b) a 2-(3′,4′,5′-trimethoxyphenyl)benzo[*d*]imidazoline (BIH) organic hydride domain,[5,10] primarily chosen because benzimidazolines are amongst the most powerful known organic donors of hydride. Benzimidazolines simultaneously exhibit the lowest energies for heterolytic cleavage of the organic hydride C–H bond (i.e., hydricity, approaching 170 kJ mol$^{-1}$) and very high nucleophilicities, which approach those of more common borohydride reagents such as $NaB(CN)H_3$;[5,10] c) a methylene 'spacer' between the ligand and organic hydride domains, providing (i) convenient synthetic access to the ligand and (ii) flexibility while retaining abutted metal and organic hydride domains.

The new ligand was designed to be integrated into novel rhodium and iridium target complexes $[Cp^*M^{III}(\mathbf{L}^{BI+})X]^{n+}$ (M = Rh, Ir), offering enhanced reactivity compared to related $[Cp^*M^{III}(diimine)X]$ centres. Electrochemical/chemical reduction of $[Cp^*M^{III}(diimine)X]$ can form the metal hydrides $[Cp^*M^{III}(diimine)H]$, reported by Steckhan and co-workers to regioselectively transfer hydride to NAD(P)$^+$.[11] Fish and co-workers reported that coordination of the nicotinamide amide group to the $[Cp^*(diimine)M^{III}H]$ intermediate facilitated the regioselective hydride transfer to afford the 1,4-dihydronicotinamide product.[5,12] The $[Cp^*M^{III}(diimine)X]$ (X = halide or solvent) complexes are now catalysts of choice for regeneration of NAD(P)H and are often incorporated into multipart systems to drive enzymatic transformations.[5,13]

Furthermore, Matsubara, Muckerman, Creutz, and co-workers recently demonstrated the potential of metal hydrides in intermolecular regeneration of benzimidazoline organic hydride donors.[14] They revealed that $[(tpy)Ru(bpy)H]^+$ (tpy = 2,2′:6′,2″-terpyridine; bpy = 2,2′-bipyridine) regioselectively transfers hydride to 1,3-dimethylbenzimidazolium ion in acetonitrile solution to afford the corresponding 1,3-dimethylbenzimidazoline. Intramolecular hydride transfer should be kinetically more efficient, since the hydride and acceptor are held in close proximity. Notably, whereas $[(tpy)Ru(bpy)H]^+$ is readily isolated and crystallised, $[Cp^*M(diimine)H]^+$ (M = Rh, Ir) species are much more reactive, the Rh–H species being difficult to observe spectroscopically, let alone to isolate.[15] Therefore, the prospect of efficient intramolecular transfer of hydride from metal to benzimidazolium in the target species appeared excellent.

Scheme 2b depicts the desirable synergic cooperativity between the metal and organic hydride centres that was anticipated for the target complexes. It was expected that if ligand E in the left-side species were an unsaturated organic substrate, then metal binding would polarise and activate it to hydride addition (the solid arrow) to afford the product anion ($EH^-$) that would be released upon protonation ($[M]–EH^- + H^+ \rightarrow [M] + EH_2$). This is analogous to the catalytic centre of yADH (Scheme 2a), in which a zinc ion binds and activates the acetaldehyde substrate to transfer of hydride from NADPH; protonation then releases ethanol. It was also envisaged that if $EH^-$ in the right-side species were a donor of hydride, such as formate ($HCOO^-$) or isopropanoate ($Me_2HCO^-$), then metal-centre-mediated back-transfer of hydride from $EH^-$ to benzimidazolium ($BI^+$; the dashed arrow) would regenerate the benzimidazoline (BIH) organic hydride. Such a metal-mediated hydride transfer to the benzimidazolium cation would be akin to the hydride transfer to a pterin cofactor proposed to take place in "Fe–S free", mononuclear [Fe] hydrogenases.[1] Correspondingly, human alcohol dehydrogenase facilitates direct transfer of hydride from zinc-polarised ethanol to $NAD^+$, thereby affording acetaldehyde (leading, in excess, to hangovers) and NADH.[5,16] If both of the forward and reverse processes in Scheme 2b were coupled in the same reaction mixture, then the targeted complexes could catalyse the transfer hydrogenation of an organic substrate. Hence we made the target $[Cp^*M(\mathbf{L}^{BI})Cl]^+$ complexes and have tested their abilities as catalysts for the transfer hydrogenation of imines by formic acid/formate.

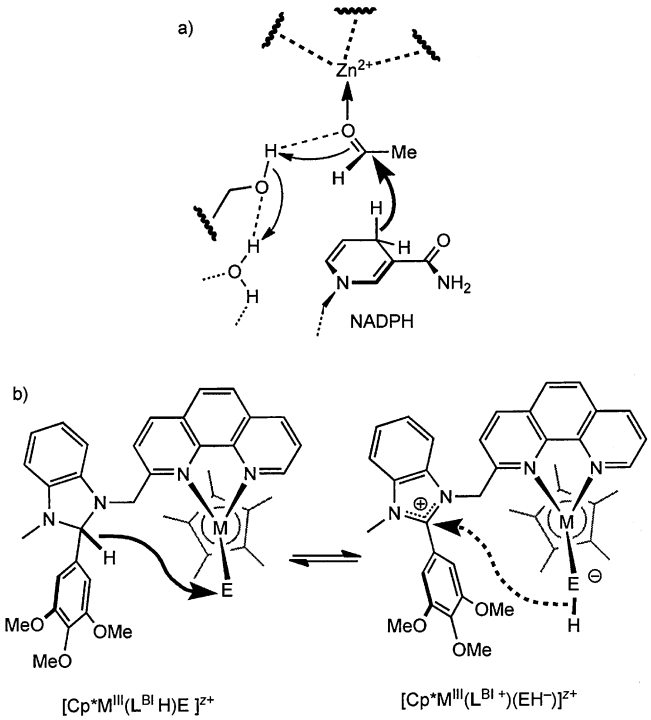


**Scheme 2.** The zinc-catalysed hydride transfer step in yeast alcohol dehydrogenases (a), which provided the inspiration for the reactivity targeted in the new metal-organic hydride conjugates made in this study (b), E = bound unsaturated substrate (e.g., imine, ketone, $CO_2$).

## Results and Discussion

### Synthesis and spectroscopy

The new ligands $[\mathbf{L}^{BI}][PF_6]$ and $\mathbf{L}^{BI}H$ were synthesised by adapting established methods (Scheme 3). Aerobic condensation of 1,2-phenylenediamine with 3,4,5-trimethoxybenzaldehyde afforded 2-(3′,4′,5′-trimethoxyphenyl)-benzimidazole,[17] which was *N*-methylated in good yield using methyl iodide and sodium hydride.[17] Reaction of the *N*-methyl benzimidazole with 2-bromomethyl-1,10-phenanthroline[18] in anhydrous ace-

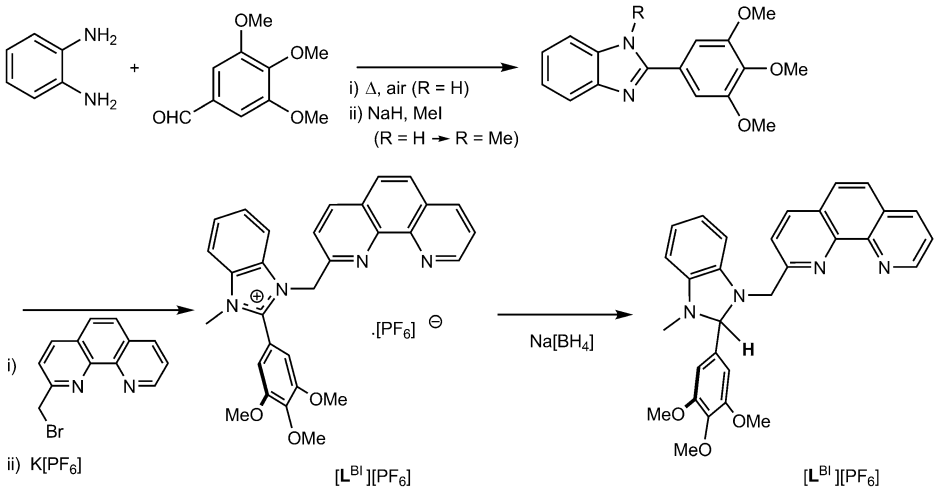


**Scheme 3.** Syntheses of $[\mathbf{L}^{BI}][PF_6]$ and $\mathbf{L}^{BI}H$.

tonitrile followed by anion metathesis using $K[PF_6]$ afforded $[\mathbf{L}^{BI}][PF_6]$ in good yield (60%) as a white crystalline solid. The corresponding phenanthroline-substituted benzimidazoline ($\mathbf{L}^{BI}H$) was obtained in near-quantitative yield from the reduction of $[\mathbf{L}^{BI}][PF_6]$ with $Na[BH_4]$ in acetonitrile. Representative $^1H$ NMR spectra of $[\mathbf{L}^{BI}][PF_6]$ and $\mathbf{L}^{BI}H$, and the X-ray crystal structure of $[\mathbf{L}^{BI}][PF_6]$ are presented in the Supporting information.

The complexes $[Cp^*M(\mathbf{L}^{BI})Cl][PF_6]_2$ (M = Rh, Ir) were obtained in excellent yield (ca. 90%) by reaction of $[\mathbf{L}^{BI}][PF_6]$ with the corresponding $[Cp^*MCl_2]_2$ precursor in acetonitrile, followed by anion metathesis using $K[PF_6]$. The complexes were characterised by $^1H$ and $^{13}C\{^1H\}$ NMR spectroscopy, FT-IR spectroscopy, ESI-HRMS, and microanalysis (see the Experimental Section). The $^1H$ NMR and $^{13}C\{^1H\}$ NMR spectra of the Rh and Ir complexes are very similar. The data for $[Cp^*Ir(\mathbf{L}^{BI})Cl]^{2+}$ are representative; of note are the doublets at $\delta = 6.89$ and 6.34 ppm for geminally coupled, inequivalent methylene protons in the $^1H$ NMR spectrum, which also shows broadened, inequivalent 2,6-phenyl and 3,5-OMe resonances of the 3,4,5-trimethoxyphenyl group at $\delta = 7.71$ and 7.60 ppm and at $\delta = 3.96$ and 3.93 ppm, respectively (see the Supporting Information, Figure 3S). The $^{13}C\{^1H\}$ NMR spectrum shows corresponding inequivalences and peak broadenings, collectively consistent with restricted rotation of the $BI^+$ group with respect to the adjacent bulky metal domain. In UV/Vis spectra of $[Cp^*Rh(\mathbf{L}^{BI})Cl]^{2+}$ and $[Cp^*Ir(\mathbf{L}^{BI})Cl]^{2+}$, the characteristic, intense, $\pi(phen) \rightarrow \pi^*(phen)$ bands appear at 279 and 282 nm, respectively, and obscure all other bands (see the Supporting Information, Figure 4S).

## X-ray crystallography

X-ray crystal structures were determined for $[\mathbf{L}^{BI}][PF_6]$ and $[Cp^*Ir(\mathbf{L}^{BI})Cl][PF_6]_2$. In the structure of the $[\mathbf{L}^{BI}]^+$ cation (see the Supporting Information, Figure 5S), the interplanar angle between the benzimidazolium and phenanthroline groups is 77°. Interestingly, the geometry apparently minimises the C2(BI)···N2(phen) distance at 2.909(2) Å (cf. sum of van der Waals radii ≈3.25 Å[19]), suggestive of a stabilising (electrostatic) interaction between the positively charged imidazolium ring and the phenanthroline lone pairs.

The crystal structure of $[Cp^*Ir(\mathbf{L}^{BI})Cl][PF_6]_2$ is centrosymmetric with both enantiomers of the axially chiral cation present. In the $[Cp^*Ir(\mathbf{L}^{BI})Cl]^{2+}$ cation (Figure 1), the $[Cp^*Ir(phen{-})Cl]^+$ and benzimidazolium centres appear splayed apart, thus minimising intramolecular electrostatic and steric interactions, and the rotamer with the 3,4,5-trimethoxyphenyl ring oriented toward the chlorido co-ligand is observed. However, the Cl-$C_{phenyl}$ distances range 3.662(7)–4.617(7) Å and are outside the sum of the van der Waals radii (ca. 3.45 Å).[19] In contrast, dissociation of chloride from $[Cp^*Rh(\mathbf{L}^{HE})Cl]^{2+}$, our previously reported Rh catalyst for imine hydrogenation, is promoted by close intramolecular aryl–chlorido ligand steric interactions.[4] The bond lengths and angles within the $[Cp^*Ir(diimine)Cl]^+$ core are within reported ranges.[15c,20,21] The $N_{phen}$-Ir-$N_{phen}$ bite angle is 77.3(2)°. Notably, the Ir–$N_{phen}$ bond lengths differ significantly, at 2.085(5) and 2.148(5) Å, with the longer Ir–N bond being that to the more sterically encumbered benzimidazolium-substituted pyridyl ring.

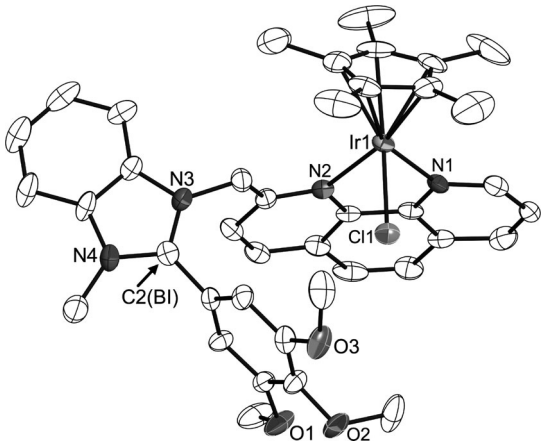


**Figure 1.** The dication from the X-ray crystal structure of $[Cp^*Ir(\mathbf{L}^{BI})Cl][PF_6]_2$ (thermal ellipsoids are set to 50% probability at 150 K; $[PF_6]^-$ anions and all H atoms are omitted for clarity). Selected distances (Å) and angles (°): Av. Ir–C(Cp*) 2.176(7), Ir–N1 2.085(5), Ir–N2 2.148(5), Ir–Cl 2.4031(16), C2(BI)···Ir 5.614(7); N1-Ir-N2 77.3(2), N1-Ir-Cl 85.92(15), N2-Ir-Cl 84.00(14).

**Table 1.** Yields for the transfer hydrogenation of imines to afford the corresponding amine using formic acid/formate as the hydride source and [Cp*Rh$^{III}$(diimine)] or [Cp*Ir$^{III}$(diimine)] complexes as the catalysts.

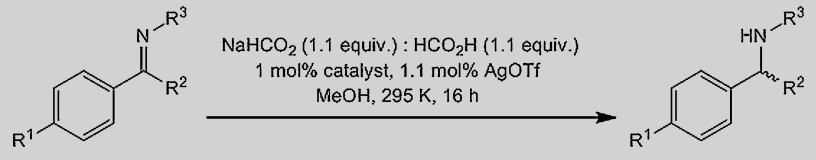


| Entry | Substrate | | | Yield [%] of product using catalyst[a] | | | |
|---|---|---|---|---|---|---|---|
| | $R^1$ | $R^2$ | $R^3$ | [Cp*Rh($\mathbf{L}^{BI}$)Cl]$^{2+}$ | [Cp*Rh$^{III}$(phen)Cl]$^{+}$ | [Cp*Ir($\mathbf{L}^{BI}$)Cl]$^{2+}$ | [Cp*Ir$^{III}$(phen)Cl]$^{+}$ |
| 1a | Cl | H | (4-Me)Ph | 71 | 7 | <1 | <1 |
| 1b | | | | 15[b] | – | – | – |
| 1c | | | | 76[c] | – | – | – |
| 1d | | | | – | 3[d] | – | – |
| 2 | Me | H | (4-Me)Ph | 88 | 13 | <1 | <1 |
| 3 | OMe | H | (4-Me)Ph | 93 | 4 | – | – |
| 4 | Cl | Me | (4-Me)Ph | 17 | 3 | – | – |
| 5a | Cl | H | Cy | 85 | <1 | – | – |
| 5b | | | | 11[b] | – | – | – |
| 6 | Cl | H | *n*Bu | 65 | 8 | – | – |

Product yields were ascertained by $^1$H NMR spectroscopy and are for 16 h reactions. Unless otherwise indicated, each reaction was performed under a dinitrogen atmosphere in 10 mL of solvent with 0.24 mmol of imine substrate. [a] Hexafluoridophosphate salts; [b] performed in air; [c] no AgOTf added; [d] 5 mol% 1,3-dimethyl-2-(3,4,5-trimethoxyphenyl)-benzo[*d*]imidazolium hexafluoridophosphate added. In all cases, no further conversion was observed upon extending the reaction time to 36 h.

### Catalytic transfer hydrogenation of imines

Complexes [Cp*M($\mathbf{L}^{BI}$)Cl]$^{2+}$ (M = Rh, Ir) and [Cp*M$^{III}$(phen)Cl]$^{+}$ (M = Rh, Ir) were screened as catalysts for the transfer hydrogenation of imines by formate/formic acid at ambient temperature (295 K). Table 1 presents the reaction conditions and the yields of amine product for each catalytic reaction attempted.

The results are revealing. First, [Cp*Rh($\mathbf{L}^{BI}$)Cl]$^{2+}$ catalysed the hydrogenation of most imines examined with yields of amine product typically >70%. The clear exception was the secondary ketimine (Table 1, entry 4). This was likely due to the increased steric bulk at the imine carbon atom hindering hydride transfer. Reactions catalysed by [Cp*Rh($\mathbf{L}^{BI}$)Cl]$^{2+}$ did not require addition of AgOTf (e.g., Table 1, entry 1c), perhaps suggestive of a labilising steric interaction between $\mathbf{L}^{BI+}$ (or $\mathbf{L}^{BI}$H) and the chlorido coligand. The longer Ir–$N_{phen}$ bond for the benzimidazolium-substituted pyridyl ring (in comparison to that to the unsubstituted pyridyl ring) in [Cp*Rh($\mathbf{L}^{BI}$)Cl]$^{2+}$ (see above) is perhaps noteworthy in this regard. Since $\mathbf{L}^{BI}$H showed only slight degradation (<5% by $^1$H NMR spectroscopy) following prolonged storage (>24 h) in air in acetone or in MeCN solutions and [Cp*Rh($\mathbf{L}^{BI}$)Cl]$^{2+}$ is air stable, the pronounced air sensitivity of the catalytic reactions (Table 1, entries 1b and 5b) suggests a Rh–H intermediate, such as [Cp*Rh$^{III}$(diimine)H]$^{+}$, that persists long enough to be destroyed by molecular dioxygen.

In contrast to [Cp*Rh($\mathbf{L}^{BI}$)Cl]$^{2+}$, the control complex [Cp*Rh(phen)Cl]$^{+}$ performed extremely poorly under identical conditions, with yields of amine typically <10%. Addition of 1,3-dimethyl-2-(3,4,5-trimethoxyphenyl)-benzo[*d*]imidazolium hexafluoridophosphate to reactions catalysed by [Cp*Rh$^{III}$(phen)Cl]$^{+}$ decreased, rather than increased, the yield of amine (Table 1, entry 1d).

No imine reduction occurred when using either [Cp*Ir($\mathbf{L}^{BI}$)Cl]$^{2+}$ or [Cp*Ir(phen)Cl]$^{+}$ as catalysts. This result concurs with expectations that the Ir$^{III}$ hydride complexes should be more stable than their rhodium analogues, consistent with [Cp*M$^{III}$(diimine)H] species being isolable for iridium, but not for rhodium.[15] The results also agree with the expectations from experiment and from theory that the hydricity—the free energy required for heterolytic cleavage of the M–H bond—should be less for a second-row metal hydride compared to its third-row metal congener,[22] and this assertion provides an explanation for the spectroelectrochemical observations that are presented below.

### Possible catalytic mechanisms

Two mechanisms that reconcile the catalysis results for the Rh complexes are diagrammatically depicted in Scheme 4:

**Pathway A** is an indirect intramolecular hydride transfer mechanism. In this pathway, substitution of the chlorido ligand in pro-catalyst [Cp*Rh($\mathbf{L}^{BI}$)Cl]$^{2+}$ by formate ion to afford [Cp*Rh($\mathbf{L}^{BI}$)(OCHO)]$^{2+}$ initiates the cycle. Elimination of $CO_2$ then gives [Cp*Rh($\mathbf{L}^{BI}$)H]$^{2+}$, which then transfers hydride intramolecularly to the benzimidazolium substituent to afford a benzimidazoline (BlH) group. The intramolecular hydride transfer opens a vacant site for coordination of imine substrate, which becomes polarised and activated on coordination to the Rh$^{III}$ centre. This is followed by back transfer of hydride from the benzimidazoline group to the bound imine substrate. Protonation of the Rh$^{III}$–amido product complex by formic acid and binding of the thus-produced formate would close the catalytic cycle. Such a mechanism is unavailable, obviously, to reactions catalysed by [Cp*Rh(phen)Cl]$^{+}$.

**Pathway B** is a direct metal-to-substrate hydride transfer mechanism. The initial steps, from precatalyst [Cp*Rh($\mathbf{L}^{BI}$)Cl]$^{2+}$ to [Cp*Rh($\mathbf{L}^{BI}$)H]$^{2+}$, are identical to those in pathway A. Then follows binding of the substrate, which could be accelerated by breaking of the longer phenanthroline–Rh bond, thereby avoiding a 20-electron intermediate. Hydride transfer to the substrate would follow, with the catalytic cycle closed by protonation of the amido product complex by formic acid and binding of the thus-formed formate, as in Pathway A.

In pathway A, the benzimidazolium/benzimidazoline group has a functional role as an organic hydride acceptor/donor. In

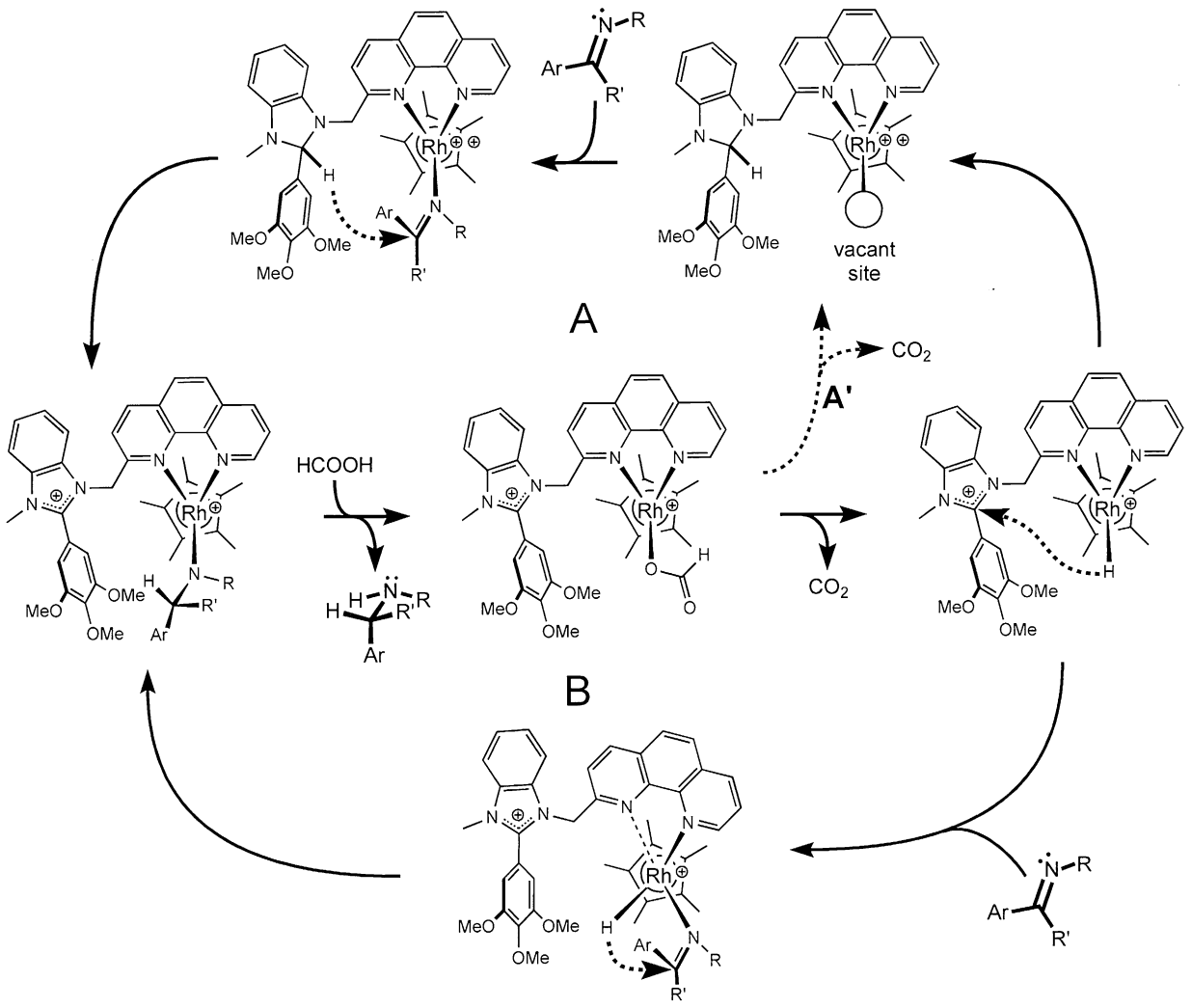


**Scheme 4.** Alternative possible mechanistic pathways for the formate-driven hydrogenation of imines catalysed by $[Cp^*Rh(\mathbf{L}^{BI})Cl]^{2+}$.

contrast, in pathway B, the benzimidazolium group serves to provide the steric bulk to weaken the Rh–phenanthroline binding. The sensitivity of reactions catalysed by $[Cp^*Rh(\mathbf{L}^{BI})Cl]^{2+}$ to air indicates that, overall, reduction of an imine substrate by $[Cp^*Rh(\mathbf{L}^{BI})H]^{2+}$ is not fast relative to reaction of this Rh–H species with molecular oxygen. This does not help to identify the major reduction pathway but does suggest that the $Rh^{III}$–H species forms in the reaction mixture.

### Cyclic voltammetry

Metal hydride formation and stability and the likelihood of hydride transfer to the benzimidazolium group were further probed by (spectro)electrochemical experiments. The cyclic voltammograms (CVs) of $[Cp^*Rh(\mathbf{L}^{BI})Cl]^{2+}$ and $[Cp^*Ir(\mathbf{L}^{BI})Cl]^{2+}$ under anhydrous conditions reveal an irreversible primary reduction process at −0.79 and −0.92 V, respectively, which gives rise to a small anodic peak in reverse sweeps at −0.63 and −0.53 V, respectively (Figure 2). CVs of $[Cp^*M^{III}(phen)Cl][PF_6]$ (M = Rh, Ir) were also recorded and show the primary reduction process at −0.85 and −0.97 V, respectively. The elec-

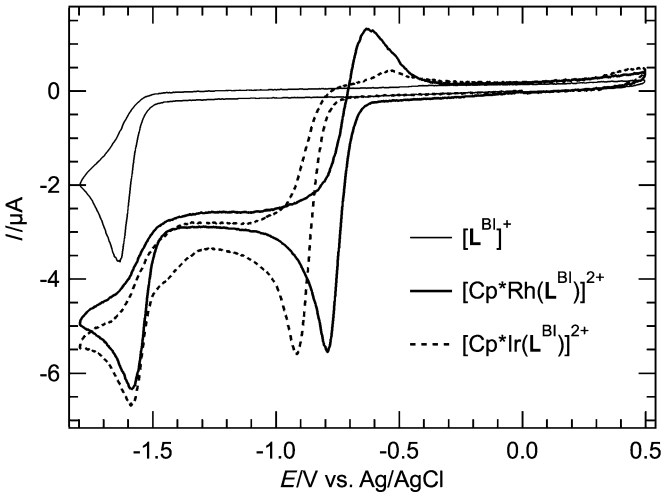


**Figure 2.** CVs of $[\mathbf{L}^{BI}][PF_6]$ (thin trace), $[Cp^*Rh(\mathbf{L}^{BI})Cl][PF_6]_2$ (bold trace), and $[Cp^*Ir(\mathbf{L}^{BI})Cl][PF_6]_2$ (dotted trace) in MeCN/0.1 M $[NBu_4][PF_6]$. Other conditions: 1.0 mm diameter glassy carbon minidisk working electrode, scan rate = 100 mV $s^{-1}$, nitrogen atmosphere, $T$ = 295 K; $E_{1/2}$ ($Fe^{II/III}$) = +0.48 V for ferrocene standard, which is +0.63 V vs. SHE.[24]

trochemical behaviour is characteristic for $[Cp^*M^{III}(diimine)Cl]^+$ (M = Rh, Ir) complexes and arises from 2-electron reduction concerted with M–Cl bond cleavage, to afford the corresponding $M^I$ species and $Cl^-$ ion [Equation (1)].[15] The peak in the reverse scan corresponds to $2e^-$-oxidation of the $M^I$ species, concerted with re-binding of a chlorido ligand, the reverse of Equation (1), or with binding of solvent **S** [Equation (2)]. The positive shifts in the primary reduction potential of $[Cp^*M(\mathbf{L}^{BI})Cl]^{2+}$ compared to the corresponding $[Cp^*M(phen)Cl]^+$ complex (by ~60 mV) result from the increased charge on the $BI^+$-substituted complexes.

$$[Cp^*M^{III}(\mathbf{L}^{BI})Cl]^{2+} + 2e^- \rightleftharpoons [Cp^*M^{I}(\mathbf{L}^{BI})]^{+} + Cl^- \quad (1)$$

$$[Cp^*M^{I}(\mathbf{L}^{BI})]^{+} + \mathbf{S} \rightarrow [Cp^*M^{III}(\mathbf{L}^{BI})(\mathbf{S})]^{3+} + 2e^- \quad (2)$$

CVs of $[Cp^*Rh(\mathbf{L}^{BI})Cl]^{2+}$ and $[Cp^*Ir(\mathbf{L}^{BI})Cl]^{2+}$ scanned to more negative potentials reveal a chemically irreversible, $1e^-$-reduction process at −1.59 V, Figure 2. These waves are not observed in the CVs of $[Cp^*M^{III}(phen)Cl][PF_6]$ (M = Rh, Ir). CVs of $\mathbf{L}^{BI+}$ over the range −1.8 to +0.5 V show a comparable irreversible reduction process at −1.63 V, Figure 2. Thus, the reduction processes at approximately −1.6 V are $BI^+$-centred. The chemical irreversibility may be attributed to rapid homocoupling of the neutral benzimidazole radical ($BI^•$) to a dibenzimidazole dimer [$\mathbf{L}^{BI}$–$\mathbf{L}^{BI}$; see the Supporting Information, Scheme 1S, and Equations (3) and (4)]. Unmediated electrochemical reduction of benzimidazolium cations under anhydrous conditions is known to afford dibenzimidazole dimer.[23] In CVs of $[Cp^*Rh(\mathbf{L}^{BI})Cl]^{2+}$ and $[Cp^*Ir(\mathbf{L}^{BI})Cl]^{2+}$ scanned to more negative potentials, consecutive reversible $1e^-$ couples are observed at $E_{1/2} = -2.10$ and −2.41 V (Rh) and at $E_{1/2} = -2.14$ and −2.46 V (Ir; see the Supporting Information, Figure 6S), which correspond to successive reductions of the phenanthroline ligand to the radical anion then dianion.[15]

$$[Cp^*M^{I}(\mathbf{L}^{BI})]^{+} + e^- \rightleftharpoons [Cp^*M^{I}(\mathbf{L}^{BI\cdot})] \quad (3)$$

$$2\,[Cp^*M^{I}(\mathbf{L}^{BI\cdot})] \rightarrow [Cp^*M^{I}(\mathbf{L}^{BI}\text{–}\mathbf{L}^{BI})M^{I}Cp^*] \quad (4)$$

CVs of the $[Cp^*M(\mathbf{L}^{BI})Cl]^{2+}$ and $[Cp^*M(phen)Cl]^+$ complexes (M = Rh and Ir) before and after addition of 10% *v/v* triethanolamine (TEOA)/TEOAH[$BF_4$] $^{MeOH}_{H_2O}$pH 7 buffer[25] in MeOH (100 mM) are presented in Figure 3. In each case, addition of buffer causes the first cathodic peak, which corresponds to the $M^{III}$–Cl/$M^I$ process [Equation (1)], to broaden and the associated anodic peak to drop in current or disappear, which is indicative of a loss of chemical reversibility. The loss of reversibility, in turn, suggests that the $M^I$ species are consumed under the more protic conditions, presumably by hydride formation

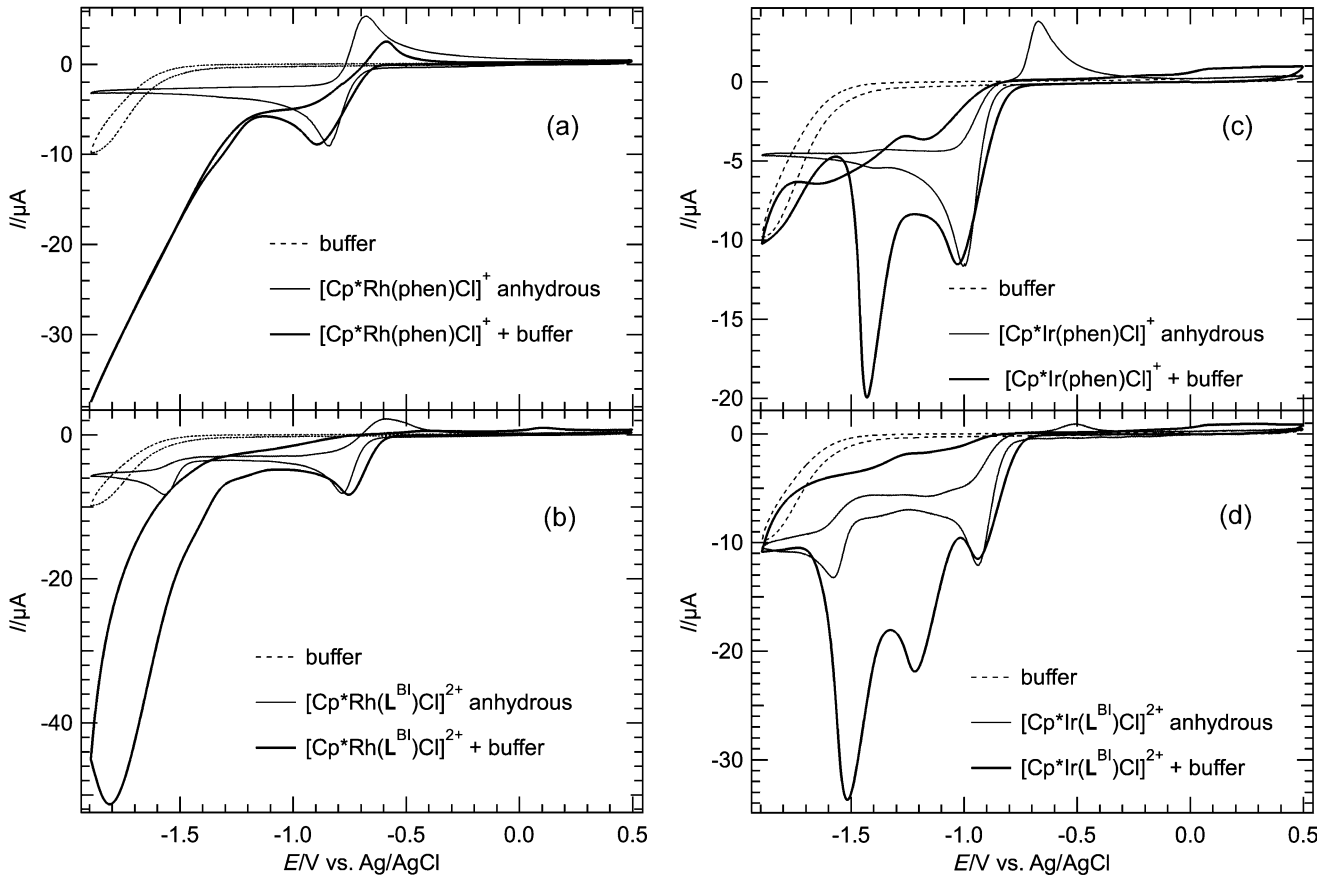


**Figure 3.** CVs of (a) $[Cp^*Rh(phen)Cl][PF_6]_2$, (b) $[Cp^*Rh(\mathbf{L}^{BI})Cl][PF_6]_2$, (c) $[Cp^*Ir(phen)Cl][PF_6]_2$ and (d) $[Cp^*Ir(\mathbf{L}^{BI})Cl][PF_6]_2$ in MeCN/0.1 M $[NBu_4][PF_6]$ before and after addition of TEOA/TEOAH $^{MeOH}_{H_2O}$pH 7 buffer in MeOH. Other conditions are as listed in the caption to Figure 2.

[Equation (5)], within the CV timescale (ca. 0.1 ms). For the Ir complexes, the CVs show new cathodic peaks at approximately −1.5 V for formation and reduction of the corresponding metal hydride centre, $[Cp^*Ir(phen–)H]^+$. In contrast, the Rh complexes show large catalytic waves consistent with catalysis of hydrogen evolution.[15c,15f,15g,15j] This observation is consistent with the $Rh^{III}$–H species being produced, but unstable to protonation and loss of molecular hydrogen in the buffered solutions on the timescale of the CV experiments.

$$[Cp^*M^{I}(\mathbf{L}^{BI})]^+ + H^+ \text{ (buffer)} \rightarrow [Cp^*M^{III}(\mathbf{L}^{BI})H]^{2+} \quad (5)$$

### UV/Vis spectroelectrochemistry

UV/Vis spectra were acquired during electrolyses of $[Cp^*Rh(\mathbf{L}^{BI})Cl]^{2+}$ and $[Cp^*Ir(\mathbf{L}^{BI})Cl]^{2+}$ at the potential for the metal-centred first reduction process in the presence of trace water (ca. 1.0 equiv added) and, in different experiments, in the presence of the TEOA/TEOAH pH 7 buffer in MeOH. The UV/Vis spectra acquired during electrolysis are presented in Figure 4 and UV/Vis spectroscopic data for complexes and electrolysis products are given in Table 2.

Upon reduction in the presence of 1 equivalent of water, UV/Vis spectra for $[Cp^*Rh(\mathbf{L}^{BI+})Cl]^{2+}$ (Figure 4a) and $[Cp^*Ir(\mathbf{L}^{BI+})Cl]^{2+}$ (Figure 4b) transform to those for new species with peaks at 278 and 450 nm and at 285 and 461 nm, respectively. Shoulders are observed at 269 and 300 nm and at 300 and 337 nm for the reduction products of $[Cp^*Rh(\mathbf{L}^{BI})Cl]^{2+}$ and $[Cp^*Ir(\mathbf{L}^{BI})Cl]^{2+}$, respectively. Constant absorbance points, ostensibly isosbestic points (see below), are observed at 213,

**Table 2.** Wavelength and extinction coefficient data for $[Cp^*Rh(\mathbf{L}^{BI})Cl]^{2+}$ and $[Cp^*Ir(\mathbf{L}^{BI})Cl]^{2+}$ and the primary product(s) of exhaustive reductive electrolysis in acetonitrile/0.1 M $[NBu_4][PF_6]$.

| | $\lambda_{max}$ [nm] ($\varepsilon_{max}$ [$10^3 \times M^{-1}$ $cm^{-1}$]) | |
|---|---|---|
| | $[Cp^*Rh(\mathbf{L}^{BI})Cl]^{2+}$ | $[Cp^*Ir(\mathbf{L}^{BI})Cl]^{2+}$ |
| Starting complex | 206 (71), 279 (38), 303 sh (15) | 207 (71), 282 (34), 305, sh (17), 338 sh (5) |
| Reduction product (1 equiv water present) | 216 sh (61), 278 (33), 269 sh, 300 sh, 450 br (6.7) | 205 (62), 285 (26), 300 sh (21), 337 sh (8), 461 (5.1) |
| Reduction product ($^{MeOH}_{H_2O}$pH 7 buffer added) | 274 (34), 364 sh (1.2) | 250 sh (38), 283 (30), 334 sh (9), 454 (4.0) |

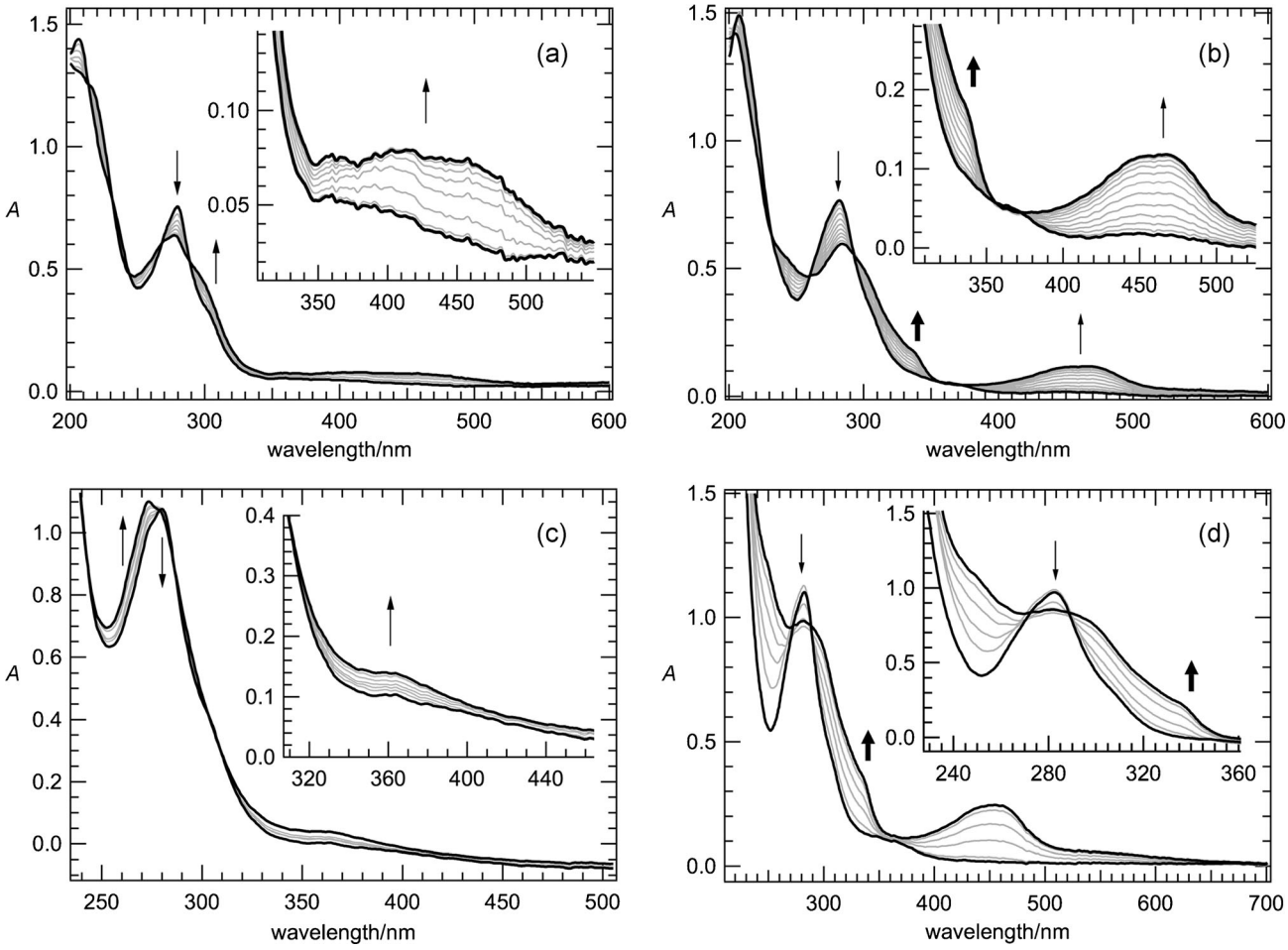


**Figure 4.** UV/Vis spectra acquired using an optically transparent thin-layer electrolysis cell during reduction of $[Cp^*Rh(\mathbf{L}^{BI})Cl]^{2+}$ at −0.75 V (a, c) and of $[Cp^*Ir(\mathbf{L}^{BI})Cl]^{2+}$ at −0.85 V (b, d) in MeCN/0.1 M $[NBu_4][PF_6]$ containing approximately 1.0 equivalent of water (a, b) or 10% *v/v* TEOA/TEOAH$[BF_4]$, $^{MeOH}_{H_2O}$pH 7 buffer in MeOH (c, d). Arrows mark the direction of change.

231, 244 and 268 nm and at 232, 260, 293 and 357 nm, respectively. The UV/Vis spectroscopic changes were accompanied by a change in the colour of the solutions from yellow to deep orange, which is consistent with the product species containing a $M^{III}$ centre and not a {Cp*$M^{I}$(diimine)} centre, as these display an intense absorption band at $>500$ nm and exhibit a distinctive deep blue colour.[15] The broad visible absorption bands at around 400–450 nm for the Rh reduction product(s) and at around 430–480 nm for the Ir reduction product(s) are characteristic for a metal hydride species of the type [Cp*M(diimine)H]. That the bands are very weak for the Rh reduction suggests the more reactive Rh–H species decomposes as the electrolysis proceeds. Protonation by water and evolution of molecular hydrogen is likely, and in the unbuffered solution would lead to build-up of the hydroxo–$Rh^{III}$ product species according to Equations (6) and (7):

$$[Cp^*Rh^{I}(\mathbf{L}^{BI})]^{+} + H_2O \rightarrow [Cp^*Rh^{III}(\mathbf{L}^{BI})H]^{2+} + OH^{-} \quad (6)$$

$$[Cp^*Rh^{III}(\mathbf{L}^{BI})H]^{2+} + H_2O \rightarrow [Cp^*Rh^{III}(\mathbf{L}^{BI})(OH)]^{2+} + {}^{1}/_{2}H_2 \quad (7)$$

Protonation of $[Cp^*Rh(\mathbf{L}^{BI})(OH)]^{+}$ and substitution of the resulting aqua species by solvent would lead to a product mixture that also contains $[Cp^*Rh(\mathbf{L}^{BI})(\mathbf{S})]^{2+}$ ($\mathbf{S}=H_2O$, MeCN) species, which could account for the obvious shoulders to the phenanthroline-centred $\pi$–$\pi^*$ band at approximately 280 nm. The same reactions likely also occur, but to a lesser extent, for the less reactive $Ir^{III}$–H product, which builds in the solution and gives rise to the more intense visible band(s) between 400 and 500 nm. Thus, the primary reduction appears to ultimately afford a mixture of [Cp*$M^{III}$(diimine)X] products that includes far less $M^{III}$–H species for Rh than Ir.

The reduction of $[Cp^*Rh(\mathbf{L}^{BI})Cl]^{2+}$ and $[Cp^*Ir(\mathbf{L}^{BI})Cl]^{2+}$ in the presence of TEOA/TEOAH $^{MeOH}_{H_2O}$pH 7 buffer to prevent accumulation of hydroxide ion was also monitored by UV/Vis spectroscopy (Figure 4c,d). The UV/Vis spectroelectrochemistry for $[Cp^*Rh(\mathbf{L}^{BI})Cl]^{2+}$ (Figure 4c) reveals clean conversion to $[Cp^*Rh(\mathbf{L}^{BI})(MeCN)]^{3+}$ without any build-up of intermediates such as $[Cp^*Rh^{III}(phen–)H]$ or $\{Cp^*Rh^{I}(phen–)\}$ species.[15] The final UV/Vis spectrum after exhaustive electrolysis (i.e. when no further changes were observed) at the potential for metal-centred reduction was indistinguishable from that of $[Cp^*Rh(\mathbf{L}^{BI})(MeCN)]^{3+}$ (generated in situ by addition of AgOTf to an acetonitrile solution of $[Cp^*Rh(\mathbf{L}^{BI})Cl]^{2+}$) recorded under the same conditions. The results clearly reveal that $[Cp^*Rh(\mathbf{L}^{BI})H]^{2+}$ is unstable to protonation and release of molecular hydrogen in $^{MeOH}_{H_2O}$pH 7 buffer. UV/Vis spectra recorded during electrolysis of $[Cp^*Ir(\mathbf{L}^{BI})Cl]^{2+}$ in buffered solution at the potential for metal-centred reduction, on the other hand, are very similar to those recorded in the presence of trace water. This result is consistent with $[Cp^*Ir^{III}(diimine)H]^{+}$ complexes being more stable towards protonation than the corresponding $Rh^{III}$–H species.[15c,f,g,j]

The UV/Vis spectrum of $\mathbf{L}^{BI}H$ alone exhibits an intense phenanthroline $\pi$–$\pi^*$ transition at 266 nm and a less intense, but still prominent, band at 316 nm from the benzimidazoline group (see the Supporting Information, Figure 4S). The $\mathbf{L}^{BI+}$ cation (as the hexafluoridophosphate salt) also exhibits a phenanthroline $\pi$–$\pi^*$ transition at 266 nm with a prominent shoulder at 279 nm from the benzimidazolium group. Consequently, the growth of the band at around 330–340 nm band in the UV/Vis spectroelectrochemistry for reduction of $[Cp^*Ir(\mathbf{L}^{BI})Cl]^{2+}$ (marked by the bold arrows in Figure 4b,d) is consistent with the formation of a benzimidazoline group; that is, with a $[Cp^*Ir(\mathbf{L}^{BI}H)X]$ product species forming, presumably by transfer of hydride from metal to the benzimidazolium group. In the UV/Vis spectra of the reduction product(s) of $[Cp^*Rh(\mathbf{L}^{BI})Cl]^{2+}$ (Figure 4a,c), clear growth of a 330–340 nm band is not observed, thus the spectra afford no information about the state of the tethered benzimidazolium/benzimidazole group. Chemical reductions of $[Cp^*Rh(\mathbf{L}^{BI})Cl]^{2+}$ lead only to decomposition (see the Experimental Section). Therefore, possible catalytic pathways, and the precise role of the tethered benzimidazolium group (if any), were addressed by a DFT study.

### Density functional theory calculations

The condensed-phase free energies for the catalytic cycles shown in Scheme 4 were modelled using DFT. We initially focused on the thermodynamic aspect of the proposed steps (Scheme 5). Pathways A and B share the same first and last steps [Equation (a1) = equation (b1); Equation (a5) = Equation (b4)] of the catalytic cycle. This last step involves the substitution of the reduction product by formic acid and is highly

| | | | |
|---|---|---|---|
| Pathway A | $[Cp^*Rh(\mathbf{L}^{BI})(HCO_2)]^{2+} \rightarrow [Cp^*Rh(\mathbf{L}^{BI})H]^{2+} + CO_2$ | -55 | (a1) |
| | $[Cp^*Rh(\mathbf{L}^{BI})H]^{2+} \rightarrow [Cp^*Rh(\mathbf{L}^{BI}H)]^{2+}$ | +61 | (a2) |
| | $[Cp^*Rh(\mathbf{L}^{BI}H)]^{2+}$ + imine $\rightarrow [Cp^*Rh(\mathbf{L}^{BI}H)(imine)]^{2+}$ | -8 | (a3) |
| | $[Cp^*Rh(\mathbf{L}^{BI}H)(imine)]^{2+} \rightarrow [Cp^*Rh(\mathbf{L}^{BI})(amide)]^{2+}$ | -4 | (a4) |
| | $[Cp^*Rh(\mathbf{L}^{BI}H)(amide)]^{2+} + HCO_2H \rightarrow [Cp^*Rh(\mathbf{L}^{BI})(HCO_2)]^{2+}$ + amine | -89 | (a5) |
| Pathway B | $[Cp^*Rh(\mathbf{L}^{BI})(HCO_2)]^{2+} \rightarrow [Cp^*Rh(\mathbf{L}^{BI})H]^{2+} + CO_2$ | -55 | (b1=a1) |
| | $[Cp^*Rh(\mathbf{L}^{BI})H]^{2+}$ + imine $\rightarrow [Cp^*Rh(\mathbf{L}^{BI})(H)(imine)]^{2+}$ | +113 | (b2) |
| | $[Cp^*Rh(\mathbf{L}^{BI})(H)(imine)]^{2+} \rightarrow [Cp^*Rh(\mathbf{L}^{BI})(amide)]^{2+}$ | -64 | (b3) |
| | $[Cp^*Rh(\mathbf{L}^{BI}H)(amide)]^{2+} + HCO_2H \rightarrow [Cp^*Rh(\mathbf{L}^{BI})(HCO_2)]^{2+}$ + amine | -89 | (b4=a5) |

**Scheme 5.** DFT condensed-phase reaction free energies (kJ mol$^{-1}$) for the steps shown in Scheme 4. Imine = PhN=CHPh; amide = $PhNCH_2Ph^{-}$; amine = $PhHNCH_2Ph$.

exergonic, which provides a strong thermodynamic driving force for the overall reaction. For pathway A, all of the other steps are only mildly exergonic or mildly endergonic. In contrast, pathway B involves the formation of the relatively high-energy intermediate $[Cp^*Rh(L^{BI})(H)(imine)]^{2+}$ ($+113$ kJ mol$^{-1}$). The formation of this intermediate requires partial detachment of either the cyclopentadienyl (by $\eta^5$–$\eta^3$ ring slippage[26,27]) or the phenanthrolinyl donors,[28] in order to avoid a 20-electron intermediate (Figure 5). We find that it is the latter that gives rise to a lower energy complex. This step is then followed by the highly exergonic reduction of the coordinated imine by the metal hydride. Overall, it appears that pathway A is thermodynamically more viable, and the benzimidazolium group is vital by serving as the active hydride carrier.

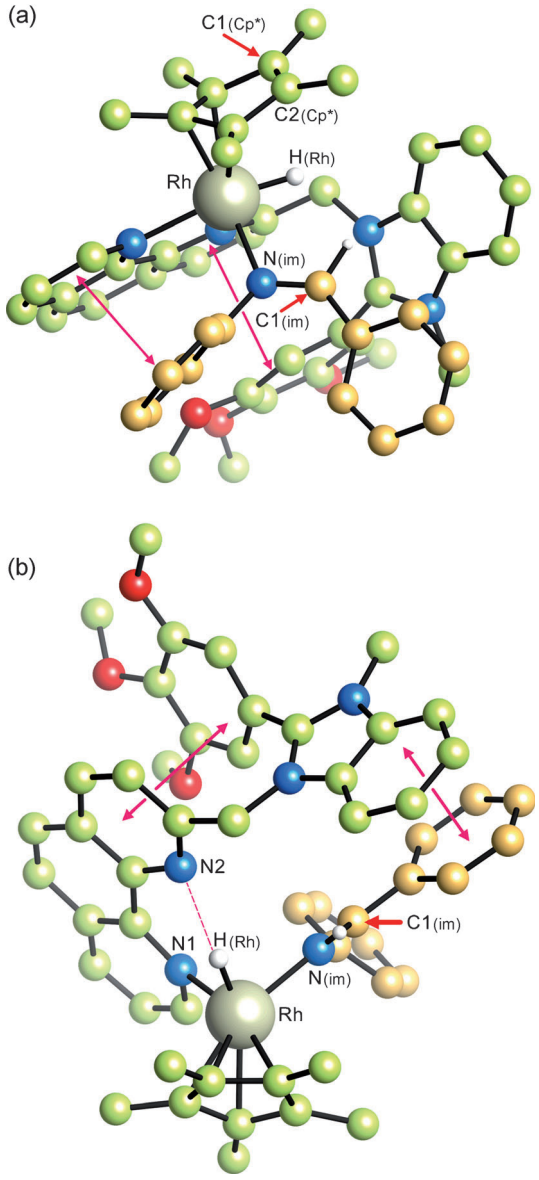


**Figure 5.** Optimised structures of the "formally" 20-electron $[Cp^*Rh(L^{BI})(H)(imine)]^{2+}$ intermediates (pathway B) with partial detachment of either (a) the cyclopentadienyl ring (bound π-allyl, off-ene structure) or (b) the phenanthrolinyl chelating ligand (the Rh···N2 distance is 3.32 Å). The calculations predict species (b) is more stable than species (a) by 45 kJ mol$^{-1}$. The C atoms of the diphenylimine substrate are coloured orange and all other C atoms are green. The double-headed arrows indicate offset inter-ring π–π stacking interactions.

Furthermore, the transition states were computed, and the full free energy reaction profile is shown in Scheme 6. The migration of the hydride from the formato ligand to the $Rh^{III}$ ion, which is common to both pathways A and B, has a barrier of 91 kJ mol$^{-1}$. Figure 6a shows the transition state for this step, in which the Rh–H bond has appreciably formed and the formato O–C–O unit has straightened. Notably, this "formally" 20-electron transition state is stabilised by partial detachment of the phenanthrolinyl donor, which may also feature in the mechanism of formate-driven regeneration of NAD(P)H catalysed by $[Cp^*Rh(bpy)(H_2O)]^{2+}$ and its close analogues.[5,11,13] The calculations suggest that the subsequent migration of the hydride from Rh to $L^{BI+}$ (Figure 6b) is determined by thermodynamics only, with no additional barrier above the $+61$ kJ mol$^{-1}$. An alternative pathway to generate $[Cp^*Rh(L^{BI}H)]^+$ is the direct hydride transfer from the formato ligand to $L^{BI+}$ (pathway A′ in Scheme 4). This step has an even larger barrier of 124 kJ mol$^{-1}$ and is therefore less favourable. After the coordination of the imine substrate, its reduction by the $L^{BI}H$ moiety has a barrier of 89 kJ mol$^{-1}$ (at 87 kJ mol$^{-1}$ on the reaction profile). In the transition state for this step (Figure 6c), the imine substrate and benzimidazoline group are aligned for direct hydride transfer. The final step is the exergonic displacement of the amine product by a formic acid molecule to regenerate the initial formato-metal complex, thus closing the catalytic cycle. In contrast, pathway B, subsequent to the generation of $[Cp^*Rh(L^{BI})H]^{2+}$, has a highest energy species at 108 kJ mol$^{-1}$ on the reaction profile for the transition state for the intramolecular hydride transfer from the metal to the imino ligand within the $[Cp^*Rh(L^{BI})(H)(imine)]^{2+}$ complex. Importantly, this transition state represents the highest point on the relevant parts of the free energy profile shown in Scheme 6. Thus, pathway A is likely to be the more favourable route for the reduction of the imine.

## Conclusion

Transfer hydrogenation has gained popularity as a reduction protocol because the use of hydrogen gas is avoided.[4,21,27,29] Herein we have demonstrated that a novel bioinspired catalyst design leads to catalysis of formate-driven reduction of imines under mild conditions (ambient temperature, 1:1 formate/formic acid buffer). Scheme 2 depicts both the inspiration, the zinc-catalysed hydride transfer step in yeast alcohol dehydrogenase (yADH), and its realisation, the key features of the catalyst system based on the $[Cp^*Rh(L^{BI})Cl]^{2+}$ precatalyst. Provided the imine substrate is not bulky at nitrogen, good to excellent yields of clean amine product were obtained.

Notably, the iridium congener, $[Cp^*Ir(L^{BI})Cl]^{2+}$, and the corresponding $[Cp^*M(phen)Cl]^+$ (M = Rh, Ir) analogues without a tethered benzimidazolium hydride acceptor, were inactive as transfer hydrogenation catalysts under identical conditions. The inactivity of the iridium complexes is due to the higher stability and lower reactivity of the Ir–H compared to the Rh–

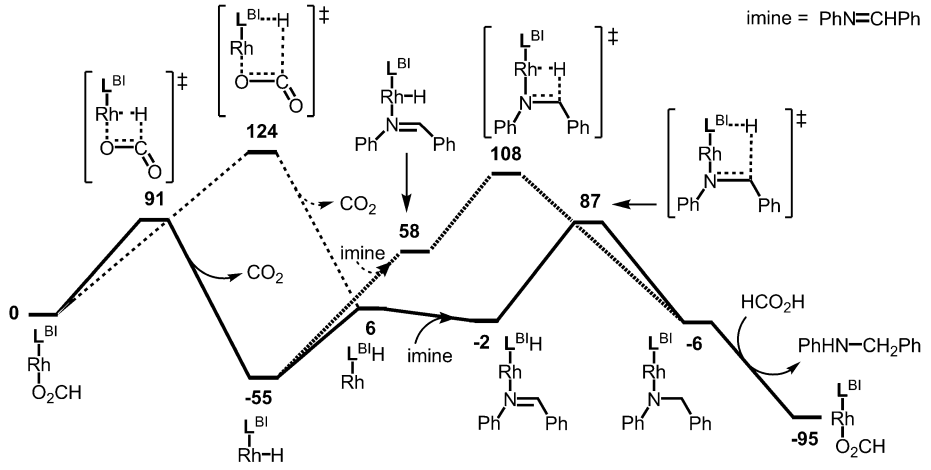


**Scheme 6.** DFT condensed-phase free energy reaction profile (kJ mol$^{-1}$): Pathway A is indicated by solid connections between species, with the alternative pathway A′ shown by thin dashes; the thicker hashed connections indicate pathway B. Energies relative to the initial formato species $[Cp^*Rh(\mathbf{L}^{BI})(HCO_2)]^{2+}$ set to 0; imine = PhN=CHPh.

H species. This was confirmed by UV/Vis spectroscopy of the Ir–H species in pH 7 buffer, conditions under which the Rh–H species rapidly decomposes (by $H_2$ evolution[15c,f,g,j]). Spectroelectrochemistry also revealed that the [Cp*M(phen–)X] cores are stable under highly reducing conditions; the spectra indicated that the Cp* and $\mathbf{L}^{BI+}$/$\mathbf{L}^{BI}$H ligands are retained. In contrast, Crabtree and co-workers recently reported that $[Cp^*Ir(\mathbf{L}^2)H]^+$ ($\mathbf{L}^2$ = 2,2′-bipyridine or two 1,3-dimethylimidazolylidene NHC ligands) catalyses transfer hydrogenation of ketones driven by isopropanol

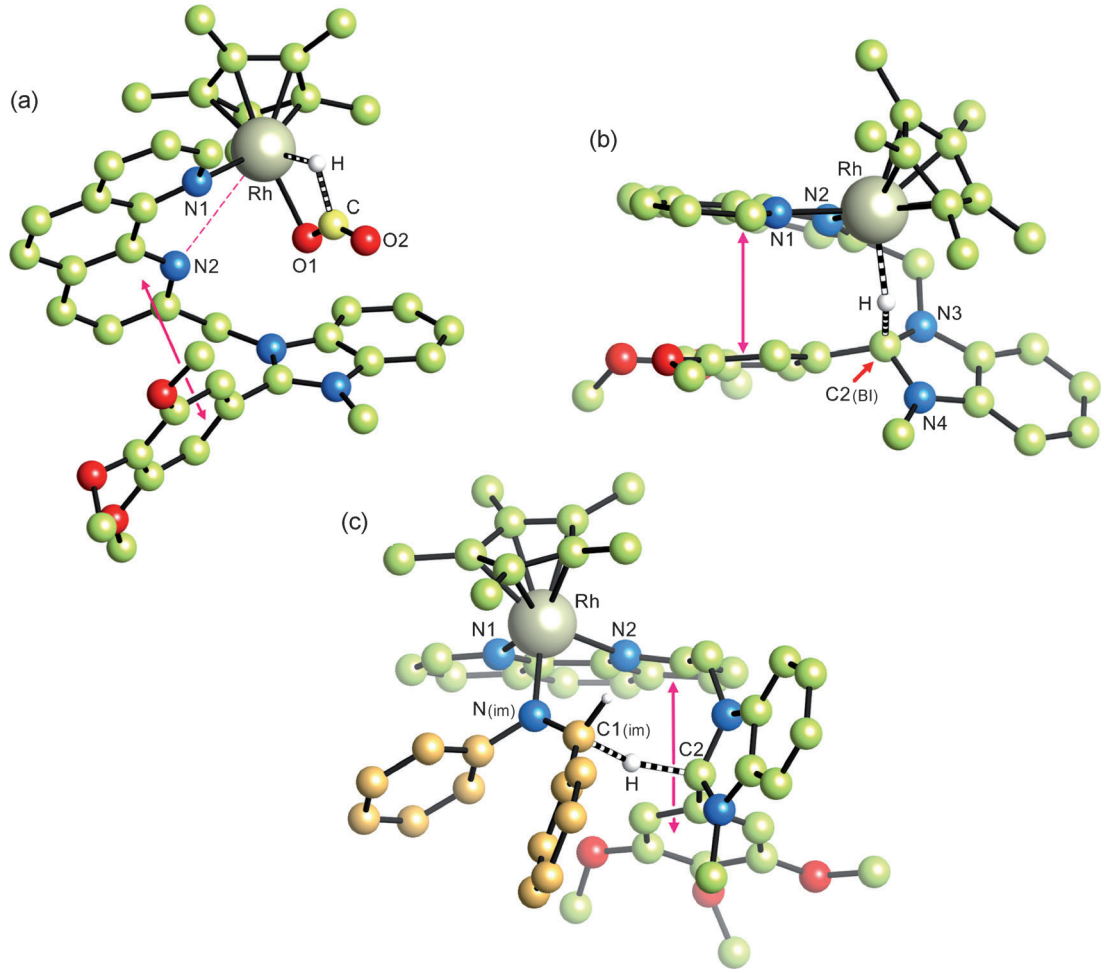


**Figure 6.** Optimised structures of the transition states in the key hydride transfer steps: a) From Rh-bound formate to metal (common to pathways A and B); b) from Rh to the tethered benzimidazolium group; c) back from benzimidazoline to metal-activated diphenylimine substrate. Key distances (Å) and angles (°) in the transition states: For formato (yellow C atom)-to-Rh hydride transfer, view (a): Rh···N2 3.30, Rh–O1 2.20, O1–C 1.20, C–O2 1.16, C<C–>H 1.44, Rh<C–>H 1.74; O1-C-O2 146.4; for Rh-to-benzimidazolium hydride transfer, view (b): Rh···H = 2.03 Å and dist. H···C2(BI) = 1.22 Å; for benzimidazoline-to-imine (im) substrate (orange C-atoms) hydride transfer, view (c): C1(im)···C2(BI) 2.78, C1(im)–H 1.39, and C2–H 1.46. Double-headed pink arrows indicate offset inter-ring π–π stacking interactions.

under highly basic conditions (KOH) at elevated temperatures (60–80 °C).[21] They cautioned that the active catalyst under the more forcing, basic conditions may be formed by Cp* loss.[27]

The inactivity of $[Cp^*Rh(phen)Cl]^+$ identifies the tethered benzimidazolium group in $[Cp^*Rh(\mathbf{L}^{BI})Cl]^{2+}$ as being essential. The DFT calculations suggest the crucial active role for the benzimidazolium group is as a novel multi-functional "hydride-borrowing" ligand[5,30] that advantageously endows the Cp*Rh complex with new catalytic reactivity. Hydride transfer from Rh–H to the tethered benzimidazolium centre opens a site for coordination of the imine substrate, and polarisation of the imine by the metal ion activates it to back-transfer of hydride from the tethered benzimidoline donor (Scheme 2, Scheme 4 (pathway A), and Scheme 6). Interestingly, DFT calculations suggest that avoidance of 20-electron species as intermediates through the partial detachment of the diimine ligand, in this case the bulkily substituted phenanthrolinyl donor, could be a key design feature to consider in pathways for processes catalysed by such complexes.

The picture that has emerged from the DFT calculations of hydride transfer from organic hydride donor to metal-activated substrate is congruent with that for formation of the hydride transfer "tunnelling ready state" (TRS) in yADH.[16] In yADH, vibrational modes reorganise the enzyme–NADPH cofactor–acetaldehyde substrate complex so that a short hydride donor–acceptor distance ($<3.1$ Å) is reached in the TRS and tunnelling facilitates the transfer of hydride to the acetaldehyde acceptor. Tunnelling of hydride, although not explicitly considered in the present calculations, may enormously accelerate intramolecular hydride transfer reactions compared to expectations based on classical analyses of barrier heights.[16] In this regard, an interesting finding revealed by the DFT calculations of the intermediates and transition states in the present catalytic cycle is that they are stabilised by intramolecular, offset π–π stacking between the dimethoxyphenyl and methylene-substituted phenanthrolinyl rings that are almost mutually parallel, with the eclipsed portions separated by $3.3\pm0.2$ Å for all species shown in Figures 5 and Figure 6. The offset inter-ring π–π stacking preorganises the tethered benzimidazolium/benzimidazoline group for hydride transfer from the metal hydride to it (Figure 6b) or to the metal-activated substrate from it (Figure 6c).

Despite the preorganisation in the present system, the barrier for hydride transfer from the 2-aryl-benzimidazoline to metal-bound substrate is high (ca. 89 kJ mol$^{-1}$, according to the DFT calculations), principally because the reorganisation energy for conversion of a 2-aryl-benzimidazoline to a 2-aryl-benzimidazolium cation is inherently large.[5,10] The high barrier for the back transfer of hydride may throttle catalyst turnover. Currently underway are attempts to address and circumvent the issue of large reorganisation energy for the organic hydride and to introduce ligand-centred chirality into the metal catalyst.

## Experimental Section

### General methods

Solvents were taken from an Innovative Technology Pure Solvent Dispenser immediately prior to use. Commercially available reagents were used as received. $^1$H and $^{13}$C NMR spectra were recorded using a Bruker DPX 300, Bruker Avance III 500 or Bruker Avance III 600 spectrometers. High-resolution positive-mode ESI mass spectra were acquired on a Thermo-Fisher Orbitrap LTQ XL ion trap mass spectrometer using a nanospray ionisation source. Cyclic voltammograms were measured using a Pine AFCBP1 bipotentiostat. Potentials given in the text are relative to a Ag/AgCl reference electrode; the standard couple for ferrocene measured in situ gave $E_{1/2}$ ($Fe^{II/III}$) $= +0.48$ V, which is $+0.63$ V vs. SHE.[24] An airtight quartz cuvette fitted with a transparent Pt-gauze working electrode and with auxiliary and reference electrodes outside the light path was used for the spectroelectrochemical experiments. The UV/Vis spectra were recorded with a Varian Cary 50 UV/Vis spectrometer. Full details of the methods for the (spectro)electrochemical experiments can be found elsewhere.[4,31] Elemental analyses were performed by the Microanalytical Unit of the Research School of Chemistry, Australian National University, Canberra.

### Syntheses

Ligand $\mathbf{L}^{BI+}$: 2-Bromomethyl-1,10-phenanthroline[32] (1.00 g, 3.66 mmol) and 1-methyl-2-(3,4,5-trimethoxyphenyl)-1*H*-benzo[*d*]imidazole[17] (1.20 g, 4.03 mmol) were heated at reflux with stirring in dry, anaerobic acetonitrile (50 mL) overnight. The acetonitrile was removed in vacuo and the residue redissolved completely in the minimum methanol. K[$PF_6$] (sat., aq.) was added to give a red-brown amorphous precipitate. The mixture was extracted with several portions of dichloromethane. The combined organic extracts were dried over sodium sulfate, filtered and loaded directly onto a neutral alumina column. Elution with dichloromethane was continued until no more starting benzimidazole was detected by TLC analysis. Further elution with dichloromethane/acetone (4:1) afforded $[\mathbf{L}^{BI}][PF_6]$, which was crystallised from acetonitrile/ether as almost colourless prisms (1.40 g, 60%). $^1$H NMR (300 MHz, $(CD_3)_2CO$): $\delta = 9.15$ (dd, $J = 4$, 2, 1H, Ar–H), 8.57 (d, $J = 8$, 1H, Ar–H), 8.45 (dd, $J = 8$, 2, 1H, Ar–H), 8.12 (d, $J = 8$, 1H, Ar–H), 8.04 (d, $J = 8$, 1H, Ar–H), 8.03 (d, $J = 8$, 1H, Ar–H), 7.98 (s, 2H, Ar–H), 7.86 (s, 2H, Ar–H), 7.75 (dd, $J = 8$, 4, 1H, Ar–H), 7.71 (td, $J = 8$, 2, 1H, Ar–H), 7.63 (td, $J = 8$, 2, 1H, Ar–H), 6.22 (s, 2H, $CH_2$), 4.32 (s, 3H, NMe), 3.79 (s, 3H, OMe), 3.66 ppm (s, 6H, OMe); $^{19}$F{$^1$H} NMR (282.2 MHz, $(CD_3)_2CO$): $\delta = 72.60$ ppm ($J = 700$, $[PF_6]^-$); $^{13}$C{$^1$H} NMR (75.5 MHz, $(CD_3)_2CO$): $\delta = 155.03$, 154.70, 153.43, 151.39, 146.27, 146.20, 142.58, 138.63, 137.22, 133.46, 132.55, 130.17, 129.35, 128.27, 127.98, 127.84, 127.23, 124.51 122.86, 117.14, 114.32, 114.28, 109.69 ($25\times C_{aryl}$), 60.72 ($CH_2$), 56.74 (OMe), 51.86 (OMe), 33.63 (NMe); FT-IR: cm$^{-1}$ 3051 (w), 3006 (w), 2969 (w), 2943 (w), 2836 (w), 1618 (w), 1585 (m), 1557 (w), 1517 (m), 1484 (m), 1484 (m), 1474 (m), 1449 (w), 1434 (w), 1520 (m), 1354 (w), 1331 (w), 1252 (m), 1190 (w), 1130 (s), 1302 (w), 1013 (w), 996 (m), 909 (w), 839 (vs), 793 (m), 757 (m), 740 (m), 733 (w), 559 ppm (s); UV/Vis (MeCN): $\lambda_{max}$ ($\varepsilon_{max}$) = 226 (63.8), 267 (38.8), 279 nm (sh, $31\times10^3$ mol$^{-1}$ cm$^{-1}$); HRMS (ESI): *m/z* calcd for $C_{30}H_{27}N_4O_3$: 491.2078 [$M^+$]; found: 491.2062; elemental analysis calcd (%) for $C_{30}H_{27}F_6N_4O_3P$: C 56.61, H 4.28, N 8.80; found: C 56.58, H 4.29, N 8.84.

Ligand $\mathbf{L}^{BI}$H: $[\mathbf{L}^{BI}][PF_6]$ (50 mg, 0.0786 mmol) was dissolved in MeCN (1 mL) and Na[$BH_4$] (20 mg, 0.529 mmol) was added. The reaction mixture was stirred for 30 min. and then water (10 mL) was added to afford $\mathbf{L}^{BI}$H as a pale yellow solid, which was collected by filtra-

tion (35 mg, 90%). $^1$H NMR (300 MHz, $(CD_3)_2CO$): $\delta = 9.11$ (dd, $J = 5$, 2, 1H, Ar–H), 8.42 (dd, $J = 8$, 1, 1H, Ar–H), 8.29 (d, $J = 8$, 1H, Ar–H), 7.91 (d, $J = 8$, 1H, Ar–H), 7.88 (d, $J = 8$, 1H, Ar–H), 7.73 (dd, $J = 8$, 5, 1H, Ar–H), 7.68 (d, $J = 8$, 1H, Ar–H), 7.12 (s, 2H, Ar–H), 6.63 (td, $J = 8$, 1, 1H, Ar–H), 6.57 (td, $J = 8$, 1, 1H, Ar–H), 6.49 (d, $J = 8$, 1H, Ar–H), 6.47 (d, $J = 8$, 1H, Ar–H). 5.50 (s, 1H, 2-BIH), 4.63 (d, $J = 16$, 1H, $CH_2$), 4.57 (d, $J = 16$, 1H, $CH_2$), 3.80 (s, 6H, OMe), 3.61 (s, 3H, OMe), 2.59 ppm (s, 3H, NMe); UV/Vis (MeCN): $\lambda_{max}$ ($\varepsilon_{max}$) = 223 (86.7), 266 (37.2), 316 nm (br, sh, $9 \times 10^3$ mol$^{-1}$ cm$^{-1}$); HRMS (ESI): *m/z* calcd for $C_{30}H_{29}N_4O_3^+$: 493.2240 [$M + H^+$]; found: 493.2243.

[Cp*Rh(**L**$^{BI+}$)Cl][$PF_6$]$_2$: A solution of [**L**$^{BI}$][$PF_6$] (50 mg, 0.0786) in MeCN (1 mL) was added to a solution of [Cp*$RhCl_2$]$_2$ (27 mg, 0.0437 mmol) in MeCN (2 mL) at which point the colour changed from red to orange-yellow. The reaction mixture was stirred for 30 min. The crude product was precipitated with K[$PF_6$] (sat., aq.), collected by filtration and recrystallised from acetone/methanol to give [Cp*Rh(**L**$^{BI+}$)Cl][$PF_6$]$_2$ as an orange-yellow powder (74 mg, 89%). $^1$H NMR (400 MHz, $(CD_3)_2CO$): $\delta = 9.62$ (dd, $J = 5$, 1, 1H, Ar–H), 9.05 (dd, $J = 8$, 1, 1H, Ar–H), 8.86 (d, $J = 8$, Ar–H), 8.32–8.40 (m, 2H, 2×Ar–H), 8.31 (d, $J = 8$, 1H, Ar–H), 8.07 (d, $J = 8$, 1H, Ar–H), 7.76 (td, $J = 8$, 1, 1H, Ar–H), 7.66 (s, br, 1H, Ar–H), 7.64 (s, br, 1H, Ar–H), 7.57 (d, $J = 8$, 1H, Ar–H), 7.47 (td, $J = 8$, 1, 1H, Ar–H), 6.92 (d, $J = 17$, 1H, $CH_2$), 6.43 (d, $J = 17$, 1H, $CH_2$), 4.24 (s, 3H, NMe), 3.96 (s, br, 3H, OMe), 3.93 (s, br, 3H, OMe), 3.90 (s, 3H, OMe), 1.70 (Cp*–Me); $^{19}$F{$^1$H} NMR (376.3 MHz, $(CD_3)_2CO$): $\delta = 72.63$ ppm ($J = 700$, [$PF_6$]$^-$); $^{13}$C{$^1$H} NMR (100.7 MHz, $(CD_3)_2CO$): $\delta = 158.33$, 155.76, 155.66, 154.38, 153.19, 147.13, 146.68, 143.20, 141.92, 140.74, 133.49, 132.23, 131.70, 131.21, 129.04, 128.65, 128.49, 128.46, 128.37, 124.83, 116.14, 114.73, 114.60, 108.92 (25×$C_{aryl}$), 99.09 (d, $J_{C-Rh} = 4$, Cp*) 61.01 ($CH_2$), 57.04 (OMe), 53.87 (OMe), 33.86 (NMe), 9.56 (Cp*–Me); FT-IR: cm$^{-1}$ 2946 (w), 2841 (w), 1629 (w), 1587 (m), 1514 (m), 1495 (m), 1483 (s), 1472 (s), 1430 (m), 1418 (m) 1396 (m), 1378 (w), 1359 (w), 1331 (m), 1249 (m), 1233 (w), 1160 (w), 1129 (s), 1019 (m), 994 (m), 908 (w), 841 (vs), 790 (m), 760 (m), 741 (w), 724 (w), 558 ppm (s); UV/Vis (MeCN): $\lambda_{max}$ ($\varepsilon_{max}$) = 206 (71.0), 279 (37.9), 303 nm (sh, $15 \times 10^3$ mol$^{-1}$ cm$^{-1}$); HRMS (ESI): *m/z* calcd for $C_{40}H_{42}ClF_6N_4O_3PRh^+$: 909.1637 [$M^{2+} + [PF_6]^-$]; found: 909.1622; elemental analysis calcd (%) for $C_{40}H_{42}ClF_{12}N_4O_3P_2Rh.H_2O$: C 44.77, H 4.13, N 5.22; found: C 44.89, H 3.74, N 5.14.

[Cp*Ir(**L**$^{BI+}$)Cl][$PF_6$]$_2$: A solution of [**L**$^{BI}$][$PF_6$] (50 mg, 0.0786) in MeCN (1 mL) was added to a solution of [Cp*$IrCl_2$]$_2$ (35 mg, 0.0439 mmol) in MeCN (2 mL) at which point the colour changed from red to orange-yellow. The reaction mixture was stirred for 30 min. The crude product was precipitated using K[$PF_6$] (sat., aq.), collected by filtration and recrystallised from acetone/methanol to give [Cp*Ir(**L**$^{BI+}$)Cl][$PF_6$]$_2$ as pale yellow microcrystals (84 mg, 93%). $^1$H NMR (400 MHz, $(CD_3)_2CO$): $\delta = 9.59$ (dd, $J = 5$, 1, 1H, Ar–H), 9.05 (dd, $J = 8$, 1, 1H, Ar–H), 8.87 (d, $J = 8$, Ar–H), 8.42 (d, $J = 8$, 1H, Ar–H), 8.38 (dd, $J = 8$, 5, 1H, Ar–H), 8.35 (d, $J = 8$, 1H, Ar–H), 8.22 (d, $J = 8$, 1H, Ar–H), 8.21 (d, $J = 8$, 1H, Ar–H), 7.78 (td, $J = 8$, 1, 1H, Ar–H), 7.71 (s, br, 1H, Ar–H), 7.60 (s, br, 1H, Ar–H), 7.56 (d, $J = 8$, 1H, Ar–H), 7.50 (t, $J = 8$, 1, 1H, Ar–H), 6.89 (d, $J = 17$, 1H, $CH_2$), 6.34 (d, $J = 17$, 1H, $CH_2$), 4.25 (s, 3H, NMe), 3.95 (s, br, 3H, OMe), 3.90 (s, br, 3H, OMe), 3.89 (s, 3H, OMe), 1.67 (Cp*–Me); $^{19}$F{$^1$H} NMR (376.3 MHz, $(CD_3)_2CO$): $\delta = 72.63$ ppm ($J = 700$, [$PF_6$]$^-$); $^{13}$C{$^1$H} NMR (100.7 MHz, $(CD_3)_2CO$): $\delta = 158.38$, 156.30, 156.18, 154.12, 153.85, 149.10, 148.37, 143.78, 142.68, 141.26, 134.10, 132.96, 132.22, 131.86, 129.77, 129.50, 129.34, 129.07, 128.98, 125.28, 116.61, 115.25, 115.11, 109.46, 109.31 (25×$C_{aryl}$), 91.79 (Cp*), 61.55 ($CH_2$), 57.55 (OMe), 55.21 (OMe), 34.39 (NMe), 9.86 ppm (Cp*–Me); FT-IR: cm$^{-1}$ 2947 (w), 2846 (w), 1621 (w), 1586 (m), 1514 (m), 1496 (m), 1481 (s), 1472 (s), 1431 (w), 1418 (m), 1359 (w), 1332 (m), 1251 (m), 1232 (w), 1162 (w), 1128 (s), 1029 (w), 995 (w), 909 (w), 841 (vs), 791 (w), 763 (w), 740 (w), 721 (w), 558 (s); UV/Vis (MeCN): $\lambda_{max}$ ($\varepsilon_{max}$) = 207 (70.7), 282 (34.4), 305 (sh, 17), 338 nm (sh, $5 \times 10^3$ mol$^{-1}$ cm$^{-1}$); HRMS (ESI): *m/z* calcd for $C_{40}H_{42}ClF_6N_4O_3PIr^+$: 999.2211 [$M^{2+} + [PF_6]^-$]; found: 999.2189; elemental analysis calcd (%) for $C_{40}H_{42}ClF_{12}N_4O_3P_2Ir.H_2O$: C 41.33, H 3.82, N 4.82; found: C 41.51, H 3.52, N 4.79.

### Chemical reduction

Separate chemical reductions of [Cp*Rh(**L**$^{BI}$)Cl][$PF_6$]$_2$ were performed using excess formate ion, sodium cyanoborohydride, and sodium borohydride in [$D_4$]MeOH and in [$D_5$]MeCN. The reactions were monitored by NMR spectroscopy. In all cases, the $^1$H NMR spectra of the reaction solution revealed complicated mixtures to have formed, and clear information about formation of rhodium hydride intermediates or species with benzimidazoline groups was not obtained. Individual compounds could not be isolated from the reaction mixtures by crystallisation or, for several reactions on a larger scale, through use of conventional chromatographic techniques.

### Transfer hydrogenation catalysis

A 1:1 sodium formate/formic acid solution was made as follows; sodium formate (17.95 g, dried at 110 °C for 1 h before use, 0.264 mol) and formic acid (13.81 g, 88% in water, 0.264 mol) were placed in a 1.00 L volumetric flask and made up to volume with MeOH. The solution was shaken until the sodium formate was completely dissolved.

Imine (0.240 mmol), metal catalyst (0.0024 mmol), and silver triflate (0.0026 mmol) were combined in a Schlenk flask and dissolved in MeOH (9.00 mL). The solution was deaerated with a steady stream of dinitrogen for approximately 10 minutes, at which point a portion of the methanolic solution of 1:1 formic acid/sodium formate (1.00 mL, 0.530 mmol total) was injected. The solution was purged with high-purity nitrogen for 5 min., at which point the flask was sealed under nitrogen. Aliquots were taken at various intervals, the MeOH removed, the residue taken up in $CDCl_3$ and analysed by $^1$H NMR spectroscopy. The NMR spectra revealed the reaction mixtures contained no side-products and so yields could be calculated from the integrals of the NMR signals using the formula: (% amine)/(% amine + % imine)×100. Representative NMR spectra are presented in the Supporting Information, Figure 7S.

### X-ray crystallography

The X-ray diffraction measurements for [**L**$^{BI}$][$PF_6$] and [Cp*Ir(**L**$^{BI}$)Cl][$PF_6$]$_2$ were carried out on a Bruker Kappa II CCD diffractometer at 150 K by using graphite-monochromated $Mo_{K\alpha}$ radiation ($\lambda$ = 0.710723 Å). Symmetry-related absorption corrections using the program SADABS[33] were applied and the data were corrected for Lorentz and polarisation effects using Bruker APEX2 software.[34] The structures were solved by direct methods and the full-matrix least-squares refinement was carried out using SHELXL.[35] Non-hydrogen atoms were refined anisotropically.

### Computational methods

Standard density functional theory calculations were carried out with Gaussian 09.[36] Geometries were optimised with the M06L procedure[37] in conjunction with the def2-SVP basis set[38] Following each geometry optimisation, harmonic frequency analysis was carried out to confirm the nature of the stationary point as a minimum or a transition state. The reaction profile was examined using

17 DFT and double-hybrid DFT procedures in conjunction with the def2-TZVP basis set, and considerable variations in the quantitative values of individual relative energies were found (see the Supporting Information). In particular, for these systems which have reasonably large ligands, the inclusion of dispersion corrections lead in some cases to large changes in the relative energies. However, the qualitative picture, in particular the relative favourability of the two mechanistic pathways, is not altered by a change in the functional. The presented free energies are the average results from the four DFT procedures we deem to be the most robust for transition metal reactions, after consideration of the results of several recent benchmark studies.[39] The functionals are M06L,[37] M06,[40] PW6-B95[41] and PW6-B95-D3[42] (highlighted in bold in Table 1S, Supporting Information). To obtain zero-point vibrational energies, 298 K thermal corrections for enthalpies and entropies, M06L/def2-SVP harmonic vibrational frequencies scaled by 0.978 were used.[43] Solvation energies were obtained using the IEFPCM continuum model[44] at the B3-LYP/def2-SVP level. The parameters for methanol were used in the solvation energy calculations to reflect experimental conditions. Calculations were also performed with acetonitrile as the solvent. The solvation of the various species and so their overall free energies were near identical in both solvents ($\pm$ 2 kJ mol$^{-1}$; see the Supporting Information, Table 2S).

## Acknowledgements

We thank the Australian Research Council for funding (DP130103514). This research was undertaken with the assistance of resources provided at the NCI National Facility in Canberra and INTERSECT, which are supported by the Australian Government.

**Keywords:** biomimetic systems · density functional calculations · hydrides · ligand design · transfer hydrogenation

[1] a) S. Shima, O. Pilak, S. Vogt, M. Schick, M. S. Stagni, W. Meyer-Klaucke, E. Warkentin, R. K. Thauer, U. Ermler, *Science* **2008**, *321*, 572 – 575; b) M. J. Corr, J. A. Murphy, *Chem. Soc. Rev.* **2011**, *40*, 2279 – 2292; c) C. Tard, C. J. Pickett, *Chem. Rev.* **2009**, *109*, 2245 – 2274.

[2] N. Pollak, C. Dolle, M. Ziegler, *Biochem. J.* **2007**, *402*, 205 – 218.

[3] a) S. R. Billeter, S. P. Webb, P. K. Agarwal, T. Iordanov, S. Hammes-Schiffer, *J. Am. Chem. Soc.* **2001**, *123*, 11262 – 11272; b) J. H. Hurley, A. M. Dean, D. E. Koshland, R. M. Stroud, *Biochemistry* **1991**, *30*, 8671 – 8678; c) V. Leskovac, S. Trivic, D. Pericin, *FEMS Yeast Res.* **2002**, *2*, 481 – 494; d) R. Dumas, V. Biou, F. Halgand, R. Douce, R. G. Duggleby, *Acc. Chem. Res.* **2001**, *34*, 399 – 408; e) V. Biou, R. Dumas, C. CohenAddad, R. Douce, D. Job, E. P. Peyroula, *EMBO J.* **1997**, *16*, 3405 – 3415.

[4] A. McSkimming, M. M. Bhadbhade, S. B. Colbran, *Angew. Chem. Int. Ed.* **2013**, *52*, 3411 – 3416; *Angew. Chem.* **2013**, *125*, 3495 – 3500.

[5] A. McSkimming, S. B. Colbran, *Chem. Soc. Rev.* **2013**, *42*, 5439 – 5488.

[6] A. McSkimming, PhD Thesis, UNSW, **2013**.

[7] A. Bencini, V. Lippolis, *Coord. Chem. Rev.* **2010**, *254*, 2096 – 2180.

[8] A. McSkimming, S. Shrestha, M. M. Bhadbhade, P. Thordarson, S. B. Colbran, *Chem. Asian J.* **2014**, *9*, 136 – 145.

[9] A. McSkimming, V. Diachenko, R. London, K. Olrich, C. J. Onie, M. M. Bhadbhade, M. P. Bucknall, R. W. Read, S. B. Colbran, *Chem. Eur. J.* **2014**, *20*, 11445 – 11456.

[10] a) X. Q. Zhu, M. T. Zhang, A. Yu, C. H. Wang, J. P. Cheng, *J. Am. Chem. Soc.* **2008**, *130*, 2501 – 2516; b) D. Richter, Y. Tan, A. Antipova, X. Q. Zhu, H. Mayr, *Chem. Asian J.* **2009**, *4*, 194; c) X. Q. Zhu, Y. Tan, C. T. Cao, *J. Phys. Chem. B* **2010**, *114*, 2058 – 2075.

[11] a) R. Ruppert, S. Herrmann, E. Steckhan, *Tetrahedron Lett.* **1987**, *28*, 6583 – 6586; b) R. Ruppert, S. Herrmann, E. Steckhan, *J. Chem. Soc. Chem. Commun.* **1988**, 1150 – 1151; c) E. Steckhan, S. Herrmann, J. Thoemmes, C. Wandrey, R. Ruppert, *Angew. Chem.* **1990**, *102*, 445 – 447; d) E. Steckhan, S. Herrmann, R. Ruppert, E. Dietz, M. Frede, E. Spika, *Organometallics* **1991**, *10*, 1568 – 1577; e) D. Westerhausen, S. Herrmann, W. Hummel, E. Steckhan, *Angew. Chem. Int. Ed. Engl.* **1992**, *31*, 1529 – 1531; *Angew. Chem.* **1992**, *104*, 1496 – 1498; f) F. Hollmann, A. Schmid, E. Steckhan, *Angew. Chem. Int. Ed.* **2001**, *40*, 169 – 171; *Angew. Chem.* **2001**, *113*, 190 – 193.

[12] a) J. Lutz, F. Hollmann, T. V. Ho, A. Schnyder, R. H. Fish, A. Schmid, *J. Organomet. Chem.* **2004**, *689*, 4783 – 4790; b) H. C. Lo, R. H. Fish, *Angew. Chem. Int. Ed.* **2002**, *41*, 478 – 481; *Angew. Chem.* **2002**, *114*, 496 – 499; c) H. C. Lo, O. Buriez, J. B. Kerr, R. H. Fish, *Angew. Chem. Int. Ed.* **1999**, *38*, 1429 – 1432; *Angew. Chem.* **1999**, *111*, 1524 – 1527.

[13] a) F. Hollmann, I. W. C. E. Arends, K. Buehler, *ChemCatChem* **2010**, *2*, 762 – 782; b) T. Quinto, V. Kohler, T. R. Ward, *Top. Catal.* **2014**, *57*, 321 – 331.

[14] J. T. Muckerman, P. Achord, C. Creutz, D. E. Polyansky, E. Fujita, *Proc. Natl. Acad. Sci. USA* **2012**, *109*, 15657 – 15662.

[15] a) U. Kölle, M. Gratzel, *Angew. Chem. Int. Ed. Engl.* **1987**, *26*, 567 – 570; *Angew. Chem.* **1987**, *99*, 572 – 574; b) U. Kölle, B. S. Kang, P. Infelta, P. Comte, M. Gratzel, *Chem. Ber.* **1989**, *122*, 1869 – 1880; c) M. T. Youinou, R. Ziessel, *J. Organomet. Chem.* **1989**, *363*, 197 – 208; d) M. Ladwig, W. Kaim, *J. Organomet. Chem.* **1991**, *419*, 233 – 243; e) M. Ladwig, W. Kaim, *J. Organomet. Chem.* **1992**, *439*, 79 – 90; f) C. Caix, S. Chardon-Noblat, A. Deronzier, R. Ziessel, *J. Electroanal. Chem.* **1993**, *362*, 301 – 304; g) C. Caix, S. Chardon-Noblat, A. Deronzier, R. Ziessel, *J. Electroanal. Chem.* **1996**, *403*, 189 – 202; h) C. Caix, S. Chardon-Noblat, A. Deronzier, J.-C. Moutet, S. Tingry, *J. Organomet. Chem.* **1997**, *540*, 105 – 111; i) C. Caix, S. Chardon-Noblat, A. Deronzier, *J. Electroanal. Chem.* **1997**, *434*, 163 – 170; j) C. L. Pitman, A. J. M. Miller, *ACS Catal.* **2014**, *4*, 2727 – 2733.

[16] a) D. Roston, A. Kohen, *J. Am. Chem. Soc.* **2013**, *135*, 13624 – 13627; b) D. Roston, A. Kohen, *Proc. Natl. Acad. Sci. USA* **2010**, *107*, 9572 – 9577; c) H. H. Limbach, J. M. Lopez, A. Kohen, *Phil. Trans. R. Soc. B Biol. Sci.* **2006**, *361*, 1399 – 1415.

[17] H. Kadri, C. S. Matthews, T. D. Bradshaw, M. F. G. Stevens, A. D. Westwell, *J. Enzyme Inhib. Med. Chem.* **2008**, *23*, 641 – 647.

[18] W. H. Sun, S. Y. Jie, S. Zhang, W. Zhang, Y. X. Song, H. W. Ma, *Organometallics* **2006**, *25*, 666 – 677.

[19] a) A. Bondi, *J. Phys. Chem.* **1964**, *68*, 441 – 451; b) R. S. Rowland, R. Taylor, *J. Phys. Chem.* **1996**, *100*, 7384 – 7391.

[20] a) R. Ziessel, M.-T. Youinou, F. Balegroune, D. Grandjean, *J. Organomet. Chem.* **1992**, *441*, 143 – 154; b) R. Ziessel, S. Noblat-Chardon, A. Deronzier, D. Matt, L. Toupet, F. Balgroune, D. Grandjean, *Acta Crystallogr. B.* **1993**, *49*, 515 – 519; c) K. Gray, M. J. Page, J. Wagler, B. A. Messerle, *Organometallics* **2012**, *31*, 6270 – 6277; d) S. Hohloch, L. Suntrup, B. Sarkar, *Organometallics* **2013**, *32*, 7376 – 7385; e) A. Takayama, T. Suzuki, M. Ikeda, Y. Sunatsuki, M. Kojima, *Dalton Trans.* **2013**, *42*, 14556 – 14567.

[21] U. Hintermair, J. Campos, T. P. Brewster, L. M. Pratt, N. D. Schley, R. H. Crabtree, *ACS Catal.* **2014**, *4*, 99 – 108.

[22] X. J. Qi, Y. Fu, L. Liu, Q. X. Guo, *Organometallics* **2007**, *26*, 4197 – 4203.

[23] J. Ludvik, F. Pragst, J. Volke, *J. Electroanal. Chem.* **1984**, *180*, 141 – 156.

[24] V. V. Pavlishchuk, A. W. Addison, *Inorg. Chim. Acta* **2000**, *298*, 97 – 102.

[25] L. G. Gagliardi, C. B. Castells, C. Rafols, M. Roses, E. Bosch, *Anal. Chem.* **2007**, *79*, 3180 – 3187.

[26] a) L. Leontyeva, R. P. Hughes, A. L. Rheingold, *Organometallics* **2007**, *26*, 5735 – 5736; b) W. Simanko, W. Tesch, V. N. Sapunov, K. Mereiter, R. Schmid, K. Kirchner, J. Coddington, S. Wherland, *Organometallics* **1998**, *17*, 5674 – 5688; c) A. Pedersen, M. Tilset, *Organometallics* **1993**, *12*, 3064 – 3068.

[27] a) J. Campos, U. Hintermair, T. P. Brewster, M. K. Takase, R. H. Crabtree, *ACS Catal.* **2014**, *4*, 973 – 985.

[28] a) F. P. Fanizzi, N. Margiotta, M. Lanfranchi, A. Tiripicchio, G. Pacchioni, G. Natile, *Eur. J. Inorg. Chem.* **2004**, 1705 – 1713; b) Z. L. Lu, C. Y. Duan, Y. P. Tian, X. Z. You, X. Y. Huang, *Inorg. Chem.* **1996**, *35*, 2253 – 2258; c) F. P. Fanizzi, M. Lanfranchi, G. Natiel, A. Tiripicchio, *Inorg. Chem.* **1994**, *33*, 3331 – 3339; d) G. W. Bushnell, K. R. Dixon, M. A. Khan, *Can. J. Chem.* **1974**, *52*, 1367 – 1376.

[29] a) S. Hashiguchi, A. Fujii, J. Takehara, T. Ikariya, R. Noyori, *J. Am. Chem. Soc.* **1995**, *117*, 7562 – 7563; b) S. Zhou, S. Fleischer, K. Junge, S. Das, D. Addis, M. Beller, *Angew. Chem. Int. Ed.* **2010**, *49*, 8121 – 8125; *Angew. Chem.* **2010**, *122*, 8298 – 8302; c) B. Štefane, F. Pozgan, *Catal. Rev. Sci. Eng.* **2014**, *56*, 82 – 174; d) R. H. Morris, *Chem. Soc. Rev.* **2009**, *38*, 2282 –

2291; e) J. S. M. Samec, J. E. Backvall, P. G. Andersson, P. Brandt, *Chem. Soc. Rev.* **2006**, *35*, 237 – 248.
[30] a) R. H. Crabtree, *New J. Chem.* **2011**, *35*, 18 – 23; b) V. K. K. Praneeth, M. R. Ringenberg, T. R. Ward, *Angew. Chem. Int. Ed.* **2012**, *51*, 10228 – 10234; *Angew. Chem.* **2012**, *124*, 10374 – 10380.
[31] a) C. Gimbert-Suriñach, M. Bhadbhade, S. B. Colbran, *Organometallics* **2012**, *31*, 3480 – 3491; b) D. G. Lonnon, S. T. Lee, S. B. Colbran, *J. Am. Chem. Soc.* **2007**, *129*, 5800 – 5801; c) S. B. Colbran, S. T. Lee, D. G. Lonnon, F. J. D. Maharaj, A. M. McDonagh, K. A. Walker, R. D. Young, *Organometallics* **2006**, *25*, 2216 – 2224.
[32] A. M. S. Garas, R. S. Vagg, *J. Heterocycl. Chem.* **2000**, *37*, 151 – 158.
[33] Bruker SADABS (2001), Bruker AXS Inc, Madison, Wisconsin, USA.
[34] Bruker APEX2 (2007), Bruker AXS Inc, Madison, Wisconsin, USA.
[35] G. M. Sheldrick, *Acta Crystallogr. A* **2008**, *64*, 112 – 122.
[36] M. J. Frisch et al. Gaussian 09, Revision D.01; Gaussian, Inc.: Wallingford CT, 2009; for the full reference, see the Supporting Information.
[37] Y. Zhao, D. G. Truhlar, *J. Chem. Phys.* **2006**, *125*, 194101 – 194118.
[38] F. Weigend, R. Ahlrichs, *Phys. Chem. Chem. Phys.* **2005**, *7*, 3297 – 3305.
[39] a) B. Chan, G. E. Ball, *J. Chem. Theory Comput.* **2013**, *9*, 2199 – 2208; b) M. Steinmetz, S. Grimme, *ChemistryOpen* **2013**, *2*, 115 – 124; c) M. K. Kesharwani, J. M. L. Martin, *Theor. Chem. Acc.* **2014**, *133*, 1452.
[40] Y. Zhao, D. G. Truhlar, *Theor. Chem. Acc.* **2008**, *120*, 215 – 241.
[41] Y. Zhao, D. G. Truhlar, *J. Phys. Chem. A* **2005**, *109*, 5656 – 5667.
[42] a) A. D. Becke, *J. Chem. Phys.* **1993**, *98*, 5648 – 5652; b) S. Grimme, J. Antony, S. Ehrlich, H. Krieg, *J. Chem. Phys.* **2010**, *132*, 154104 – 154119.
[43] I. M. Alecu, J. Zheng, Y. Zhao, D. G. Truhlar, *J. Chem. Theory Comput.* **2010**, *6*, 2872 – 2887.
[44] Y. Zhao, N. E. Schultz, D. G. Truhlar, *J. Chem. Theory Comput.* **2006**, *2*, 364 – 382.

Received: September 4, 2014
Published online on ■■ ■■, 0000

# FULL PAPER

**Inspired by the yeast** alcohol dehydrogenase-catalyzed reduction of acetaldehyde to ethanol, a new catalyst for transfer hydrogenation of imines, based on a multifunctional ligand incorporating a benzimidazolium organic hydride-acceptor domain and a 1,10-phenanthroline metal-binding domain, has been designed and realised. Theory and experiment suggest hydride transfer from an organic hydride donor is a key step in both catalyses.

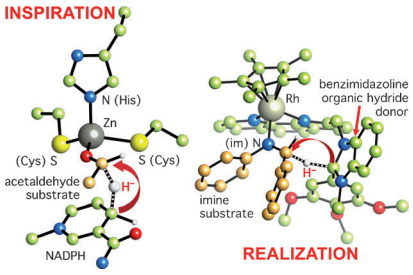


**Transfer Hydrogenation**

*A. McSkimming, B. Chan, M. M. Bhadbhade, G. E. Ball, S. B. Colbran**

■■ – ■■

**Bio-Inspired Transition Metal–Organic Hydride Conjugates for Catalysis of Transfer Hydrogenation: Experiment and Theory**


**In the final step**……of fermentation, which is catalysed by yeast alcohol dehydrogenases, hydride ion is transferred from NADPH to acetaldehyde bound and activated by the active site zinc ion; the ethanol for fine beverages results. Inspired by this biological chemistry, in their full paper on page ■■ ff., S. Colbran et al. report an artificial catalyst for the transfer hydrogenation of imines. Experiments backed by theoretical calculations suggest the mechanism of the new catalyses parallels that of the natural system.